



Résistance à la corrosion et comportement électrochimique des composites matriciels intermétalliques Fe_3Al renforcés par TiC

Mémoire

Najmeh Ahledel

**GÉNIE DES MATÉRIAUX ET DE LA MÉTALLURGIE
MAÎTRISE- AVEC MÉMOIRE**

Québec, Canada

© Ahledel, Najmeh, 2018

**Corrosion Resistance and Electrochemical
Behavior of Fe₃Al Intermetallic Matrix Composites
Reinforced by TiC**

MÉMOIRE

Najmeh Ahledeh

Sous la direction de :

Houshang Alamdari, directeur ou directrice de recherche
Hendra Hermawan, codirecteur ou codirectrice de recherche

Résumé

Le comportement à la corrosion de deux revêtements composites à matrice intermétallique Fe_3Al préparés par la technique HVOF (High Velocity Oxy Fuel) a été étudié dans une solution à 3.5% en poids de NaCl et comparé au Fe_3Al non renforcé. En outre, le chrome en tant qu'élément d'alliage utilisé dans la charge d'alimentation de HVOF pour évaluer l'effet du chrome sur le comportement à la corrosion du revêtement. Les techniques électrochimiques, y compris la polarisation potentiodynamique, le potentiel de circuit ouvert (OCP) et la spectroscopie d'impédance électrochimique (EIS) ont été considérées. La surface de l'échantillon a été analysée après la corrosion en utilisant un microscope électronique à balayage (MEB) et une spectroscopie photoélectronique par rayons X (XPS).

L'essai de potentiel en circuit ouvert a révélé qu'il existe sur le revêtement une couche d'oxyde qui pourrait être due à la technique HVOF utilisant de l'oxygène gazeux pour appliquer les revêtements. Les diagrammes de polarisation potentiométrique ont révélé que l'ajout de particules de TiC à la matrice Fe_3Al améliore les performances de corrosion de Fe_3Al , de sorte que les revêtements $\text{Fe}_3\text{Al} / \text{TiC}$ présentent un taux de corrosion légèrement 6 fois supérieur. Une spectroscopie d'impédance électrochimique a été réalisée pour étudier les mécanismes de prévention de la corrosion des revêtements et un mécanisme différent était supposé pour $\text{Fe}_3\text{Al-Cr} / \text{TiC}$.

Une analyse post-corrosion, telle que les spectres XPS et les images MEB de la couche passive, a été réalisée pour étudier la forme de corrosion. L'analyse élémentaire de la couche passive a révélé que l'addition de chrome au revêtement composite, fournit une couche passive plus protectrice en bloquant les sites d'entrée des ions chlorure.

Essais de polarisation cyclique effectués dans une solution d'acide sulfurique 0.25 M pour étudier le comportement de passivation et de piqûration de revêtements dans une solution différente pour comparer les résultats de plusieurs autres travaux sur des aluminures de fer avec Fe_3Al et deux revêtements composites de $\text{Fe}_3\text{Al} / \text{TiC}$ et $\text{Fe}_3\text{Al-Cr} / \text{TiC}$. Les résultats de la polarisation cyclique potentiodynamique ont révélé que les performances de corrosion des revêtements composites dans cette solution sont légèrement meilleures que Fe_3Al . Cependant $\text{Fe}_3\text{Al-Cr} / \text{TiC}$ présente une résistance à la piqûration inférieure à celle de deux autres revêtements.

ABSTRACT

The corrosion behavior of two Fe₃Al intermetallic matrix composite coatings (Fe₃Al/TiC and Fe₃AlCr/TiC) that prepared by high velocity oxy fuel (HVOF) technique was studied in 3.5 wt.% NaCl solution and compared with non-reinforced Fe₃Al. Furthermore, chromium as an alloying element used in the feedstock of HVOF to evaluate the effect of chromium on corrosion behaviour of the coating. Four electrochemical techniques, open circuit potential potentiodynamic polarization, and electrochemical impedance spectroscopy (EIS) were employed to examine corrosion behavior in detail. Post-corrosion analysis was done using Scanning Electron Microscopy (SEM) and X-ray Photoelectron Spectroscopy (XPS) to reveal the surface morphology and chemistry of the corroded samples.

Results from the open circuit potential test revealed that an oxide layer formed on the coating which could be due to oxidation during the HVOF coating process. The Potentiodynamic polarization graphs revealed that adding TiC particles to Fe₃Al matrix improved the corrosion performance of Fe₃Al so that the Fe₃Al/TiC coatings exhibit slightly six times more corrosion rate.

The EIS results indicated a more compact corrosion layer formed on the Cr-added coating resulting into the highest coating resistance. This is supported by the SEM/EDS and XPS analyses which revealed that a mixed oxide and hydroxide formed a passive layer. The Cr in the composite coating took the role in providing a more protective passive layer by blocking the entry sites of Cl ions. The pitting resistance of the Fe₃Al-Cr/TiC coating in 0.25 M H₂SO₄ solution was, however, lower compared to that of the two other coatings. It is concluded that the addition of TiC particles to Fe₃Al matrix, which primarily done for improving wear resistance, improves the corrosion resistance of the coating in saline solution. The addition of Cr into the Fe₃Al/TiC composite coating further improves its corrosion resistance, but the pitting resistance is not improved when tested in acid solution.

Table of Contents

Résumé.....	III
ABSTRACT.....	IV
List of Figures.....	VII
Acknowledgement.....	X
INTRODUCTION.....	1
1.1. Background.....	2
1.2. Objective.....	4
CHAPTER 1.....	5
LITERATURE REVIEW.....	5
2.1. Introduction to Mechanical Properties of Fe ₃ Al.....	6
2.1.1 Phase Diagram.....	6
2.1.2 Point defects and Dislocations.....	7
2.1.3 Mechanical Properties.....	8
2.1.4 Alloying Elements.....	9
2.1.5. Oxidation.....	9
2.2. Electrochemical Nature of Corrosion.....	10
2.2.1. Electrochemical Reactions.....	10
2.2.2. Electrochemical Thermodynamics and Electrode Potential.....	11
2.2.3. Electrochemical Kinetics of Corrosion.....	12
2.2.4. Polarization.....	13
2.2.5. Active –Passive Behavior of Fe ₃ Al.....	17
2.3. Corrosion Measurement Techniques.....	23
2.3.1. Electrochemical Methods.....	23
2.3.2. Microstructural Analyses.....	31
2.3.3. Chemical Analyses.....	32
2.4. HVOF Thermal Spray Coatings.....	34
2.5. Summary.....	35
CHAPTER 2.....	37
EXPERIMENTAL.....	37
3.1. Composite Coatings Fabrication.....	38
3.2. Preparing Samples for electrochemical tests.....	39
3.3. Operating Parameters and Solutions.....	40
3.3. Experimental Procedures.....	41
3.3.1. Open Circuit Potential Test.....	41
3.3.2. Potentiodynamic Polarization Studies.....	41
3.3.3. Electrochemical Impedance Spectroscopy (EIS).....	42
3.3.4. Energy Dispersive Spectrometry (EDS).....	42
3.3.5. X-ray Photoelectron Spectroscopy (XPS).....	42
3.3.5. Cyclic Polarization in sulphuric acid solution.....	43

CHAPTER 3	44
RESULTS AND DISCUSSION	44
4.1. Open circuit potential.....	45
4.2. Potentiodynamic polarization	46
4.3. Electrochemical impedance spectroscopy (EIS).....	47
4.4. Possible corrosion reactions.....	51
4.5. SEM and EDS Analyses	52
4.6. XPS Analysis	53
4.7. Cyclic Polarization.....	59
CONCLUSION AND OUTLOOK.....	61
5.1. General Conclusion.....	62
5.2. Outlook	63
6. References.....	65

List of Figures

- Fig. 1.** Fe-Al phase diagram. In the phase diagram, some of the solubility lines are plotted with dashed lines because they are still not well determined. Data from reference[37]..... 6
- Fig. 2.** Atomic arrangement in a B2 or D03 super-lattice; (b) Occupation probabilities of the lattice sites by Al in a Fe-Al system[2]..... 7
- Fig. 3.** (a)The influence of temperature and Al content on the yield stress of binary intermetallics (a)[45] ; (b)Stress anomaly and strain rate sensitivity of Fe–39.5 at. % Al intermetallics for a single slip system–oriented[44] 9
- Fig. 4.** The polarization of iron in acid[53] 13
- Fig. 5.** Schematic Evans diagram for the corrosion of metal M by an acid showing the application of mixed potential theory[55]..... 15
- Fig. 6.** Schematic measured polarization curve for metal M in an acid[56]..... 16
- Fig. 7.** The active-passive behaviour of a material..... 18
- Fig. 8.** Potentiodynamic polarisation curves of iron aluminide, pure Al and Fe obtained in 0.25 M H₂SO₄..... 19
- Fig. 9.** Schematic model for passivation behaviour of iron aluminide in acidic electrolyte[1].21
- Fig. 10.** Change of the open circuit potential versus time curves obtained for the Al–TiC composite sintered at (1) 900, (2) 1100, and (3) 1300 °C in 3.5% NaCl solutions[65]..... 25
- Fig. 11.** Typical Potentiostatic Anodic Polarization Plot for Type 430 Stainless Steel in 1.0 N H₂SO₄[57]..... 25
- Fig. 12.** Typical Cyclic polarization curve[70]..... 27
- Fig. 13.** A simple metal–aqueous solution interface in which the vertical dotted lines in (a) can match the electronic components determined by EIS studies[63] 29
- Fig. 14.** Example Bode plot for the equivalent circuit of Randle’s circuit[72] 30

Fig. 15. Equivalent electrical circuit model for a simple corroding electrode (left) and related Nyquist plot for the equivalent circuit (right)[72]	31
Fig. 16. XPS spectra for (a) Al and (b) Fe spectra for thermally oxidized elements at 800 °C (dotted lines) and passivated elements in 0.25 M H ₂ SO ₄ at 1 VSCE.[1]	33
Fig. 17. Schematic diagram of the high-velocity oxy-fuel spray process (HVOF)[76]	34
Fig. 18. High energy ball milling apparatus	38
Fig. 19. HVOF gun that applied the coating.....	39
Fig. 20. K0235 Flat Cell used for OCP and polarization tests	40
Fig. 21. VersaSTAT3 Potentiostat -Galvanostat workstation	41
Fig. 22. Open circuit potential of Fe ₃ Al, Fe ₃ Al/TiC and Fe ₃ Al-Cr /TiC measured for 24 hours in freely aerated 3.5 wt.% NaCl.....	45
Fig. 23. The potentiodynamic polarization curves of Fe ₃ Al, Fe ₃ Al/TiC and Fe ₃ Al-Cr/TiC in freely aerated 3.5 wt% NaCl.....	46
Fig. 24. Nyquist plot of Fe ₃ Al, Fe ₃ Al/Tic and Fe ₃ Al-Cr/TiC composite coatings after one hour immersion in 3.5% NaCl solution.....	48
Fig. 25. The proposed equivalent circuit model used to obtain impedance	49
Fig. 27. SEM micrograph and related EDS analysis of the passive layer formed on (a) Fe ₃ Al, Fe ₃ Al/TiC(b) and Fe ₃ Al-Cr/TiC (c) after potentiodynamic test exposure to 3.5% NaCl solution	53
Fig. 28. XPS Spectra for Fe 2p for (a)Fe ₃ Al (b) Fe ₃ Al/TiC and (c)Fe ₃ Al-Cr/TiC	55
Fig. 29. XPS spectra of Al 2p (a) before polarization test and (b) passivated sample	56

Fig. 30. XPS spectra of Ti2p (a) Fe ₃ Al/TiC (b) Fe ₃ Al-Cr/TiC.....	56
Fig. 31. XPS spectra of Cr 2p Fe ₃ Al-Cr/TiC	57
Fig. 32. Elemental analysis results of the surface after passivation in 3.5% NaCl solution during potentiodynamic test.....	58
Fig. 33. Cyclic polarization diagram of Fe ₃ Al, Fe ₃ Al/TiC and Fe ₃ Al-Cr/TiC coating in 0.25M sulphuric acid solution	59

Acknowledgement

My deepest gratitude goes to Professor Houshang Alamdari, my supervisor, for his constant encouragement and guidance. He accepted me as a master student while I had the responsibility of my six-month-old, breast-feed baby with two other young kids. I would like to express my appreciation to Professor Hendra Hermawan, my co-supervisor who guided me throughout this project and offered me valuable suggestions.

I also wish to acknowledge Professor Edward Ghali, Dr. Fariba Safizadeh and Nabil Sorour who have offered me valuable suggestions in the academic studies. I would also like to thank Mr. André Ferland, Mrs. Vicky Dodier, and Mr. Alain Adnot for their professional technical participation.

The last but not the least, I am a greatly indebted to my beloved husband Saeed and two sons Parsa and Daniel and my little girl Romina for their support.

INTRODUCTION

1.1. Background

Iron aluminides have received extensive attention among the most studied intermetallics since the 1930s. This is basically due to low density, high strength-to-weight ratios, ease of fabrication and resistance to high-temperature oxidation and sulfurization [1, 2]. Their application is, however, limited by their low ductility, poor creep resistance [3] and low wear resistance [4].

It has been shown that the incorporation of ceramic particles in the iron aluminide matrix improves its tribological properties. The Fe–Al/WC composite coating is an example of improvement of wear-resistance of Fe–Al coating [5, 6].

Titanium carbide (TiC), owing to its excellent mechanical, chemical and thermal properties, has been known as a good reinforcing phase to improve the mechanical properties of the aluminide matrix [7, 8]. Chen et al. [9] stated that Fe-Al intermetallics with TiC reinforcement have excellent wear resistance. These composite coatings, fabricated by laser cladding, exhibited higher resistance to dry sliding wear resistance. In addition to laser cladding, several other techniques, such as plasma spraying [10-13], wire arc spraying [14] and high-velocity oxy-fuel (HVOF) projection [15] have also been used to deposit Fe-Al alloys on carbon steels or stainless steel substrates. HVOF is a convenient process to deposit thick coatings on a variety of substrates with superior properties at low cost [16].

Although iron aluminides are mainly developed for applications at high temperatures, they also exhibit good potential for low-temperature applications. These intermetallics are a good candidate to replace stainless steel in several applications, i.e., pipes and tubes for heating elements, and main components for distillation and desalination plants [17]. A number of studies were thus concentrated on the aqueous corrosion behaviour of these materials to test the durability of these alloys in corrosive environment firstly, to examine the durability of these alloys when they are either stored ideally or during working conditions in a corrosive atmosphere. Secondly, as an alternative to conventional stainless steels.

The corrosion behaviour of iron aluminides has been studied in several acidic and basic solution [18-24]. Chiang et al. [18] studies show that Fe–Al alloys contain 3.4, 10.4, 18.7, 19.4, 29.5 and 41.7 at.% of Al. He showed that Fe-Al alloys with Al content exceeding 19 at. %, in 0.1 N H₂SO₄, have wide passivation regions with low passivation current. In addition, when the Al content of Fe–Al alloys exceeds this limit, the increment of Al content has a slight influence on passivation.

Sharma [19] compared the stability of the passive film and pitting behaviour of Fe-28Al (at. %) and Fe-28Al-3Cr (at. %) with AISI SS 304 under different pH conditions to study their performance in acidic, basic, and neutral solutions and revealed that the presence of 3 at. % Cr in iron aluminides improves the aqueous corrosion resistance and makes it comparable to AISI SS 304. Calderon et al. [20] studied the corrosion behaviour of FeAl and Fe₃Al intermetallic coatings in 1.0 M NaOH solution at room temperature and compared the performance of coatings with base alloys. Three different particle sizes were used for the coatings. The coatings were applied by two thermal spray techniques: flame spraying and HVOF. The coatings produced by the HVOF process were shown to be denser, more uniform and with lower porosity. Alloys and coatings with higher aluminum content had lower I_{corr} values and therefore greater corrosion resistance. They also reported the effect of feedstock particles size on the corrosion behaviour of the coatings. Coatings applied using medium particle size, and flame spray and those prepared using fine particle size and HVOF process were shown to be more stable [20]. Grosdidier et al. [21] investigated microstructure and corrosion properties of nanocrystalline Fe-40Al coatings by HVOF. They also showed that the feedstock powder size has a strong effect on the coating hardness by modifying the amount of hard unmelted powder particles. The electrochemical response of coatings revealed that these particles are the reason for poor corrosion resistance, compared to the bulk material. Analysis of corrosion damage showed a prevalent localized attack at intersplat boundaries or around un-melted powder particles, probably enhanced by galvanic phenomena. A mechanistic model was proposed by Rao [23] according to his investigation on repassivation of iron aluminide comparing to pure Al and Fe using a rapid scratched electrode technique in 0.25 M H₂SO₄. Few works investigated the corrosion behaviour of intermetallic matrix composites.

Amiriyani *et al.* [25] reported that the Vickers hardness and the dry sliding wear rates of Fe₃Al/TiC composite coatings at sliding speeds, ranging from 0.04 to 0.8 m s⁻¹, and under a constant load of 5 N. Wear resistance was reported to increase by increasing the TiC particles in the Fe₃Al matrix. He also compared the phase composition, microstructure, microhardness and elastic modulus of unreinforced Fe₃Al and Fe₃Al/TiC composite coatings[26]however the authors did not report the corrosion behaviour of these coatings.

Alloying elements in the form of a solid solution can also improve the mechanical or electrochemical properties of Fe-Al intermetallics [27-31]. Addition of 6 at.% chromium improves the ductility of Fe₃Al up to 10 % [32]. A few mechanisms were proposed to explain the effect of chromium on mechanical and corrosion properties of Fe₃Al. First, it has been postulated that Cr in solid solution facilitates the dislocation cross-slipping and solid solution softening[33, 34]. Epelboin et al. [35]also showed that Cr affects the surface properties through the contribution of chromium oxides to the formation of passive layers and the decrement of reaction kinetics. The decrease of water reduction reaction rate, may also lead to the reduction of hydrogen evolution and thus mitigating the hydrogen embrittlement [36].

1.2. Objective

The aim of this project can be divided into the following objectives:

1. Study the corrosion behavior of two Fe₃Al intermetallic matrix composite coatings that prepared by high velocity oxy fuel (HVOF) technique, in 3.5 wt.% NaCl solution and compared with non-reinforced Fe₃Al.
2. Evaluate the effect of adding chromium as an alloying element on passivity of Fe₃Al/TiC composite in 3.5% NaCl solution
3. Investigation of pitting tendency and passivity of Fe₃Al/TiC and Fe₃Al-Cr/TiC after passivation and compare the

Electrochemical techniques, including potentiodynamic polarization, open circuit potential and electrochemical impedance spectroscopy (EIS) are considered to examine corrosion behavior of Fe₃Al, Fe₃Al/TiC and Fe₃Al-Cr/TiC coatings. Post-corrosion analysis such as scanning electron microscopy (SEM) and x-ray photoelectron spectroscopy (XPS) are employed to characterize the passive layer which formed during polarization.

CHAPTER 1

LITERATURE REVIEW

2.1. Introduction to Mechanical Properties of Fe₃Al

2.1.1 Phase Diagram

The phase diagrams of binary iron aluminides were studied using several techniques, such as dilatometric measurement, electrical resistivity and specific heat measurement, measurement of elastic modulus and magnetic properties, X-ray diffraction methods and, more recently, the phase diagram was intensively studied with TEM [2].

Fig. 1 shows the phase diagrams for binary iron aluminides. At high temperatures, there is a solid solution of Al in Fe from 0 up to 45 at. % Al. This region at low temperatures is divided into three parts. The first part consists of disordered alloys up to 18.75 at. % Al at room temperature. At about 25 at. % Al and temperatures below 545 °C, the intermetallic phase Fe₃Al is formed. At higher Al contents the next phase is FeAl. Both Fe₃Al (D03) and FeAl (B2) phases are ordered forms on the body-centred cubic (bcc) lattice and are separated from the disordered A2 phase by first- or second-order transitions.

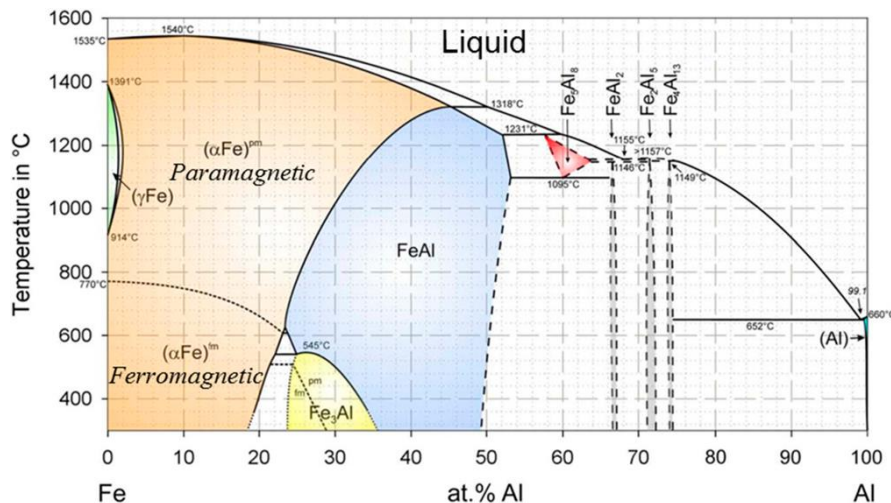


Fig. 1. Fe-Al phase diagram. In the phase diagram, some of the solubility lines are plotted with dashed lines because they are still not well determined. Data from reference [37]

The distribution of iron and aluminum atoms in the crystal lattice of FeAl (B2) and Fe₃Al (D03) phases have been studied by the X-ray diffraction method [38-40]. As presented in **Fig. 2**, in the FeAl (B2) crystal lattice, in the stoichiometric composition, Al atoms occupy the body center

sublattices (β and γ) and the Fe atoms occupy the corner sites (α sublattice). In the Fe_3Al (D03) structures, however, the Fe atoms occupy both α and β sublattices, while the Al atoms occupy the γ sublattice [41].

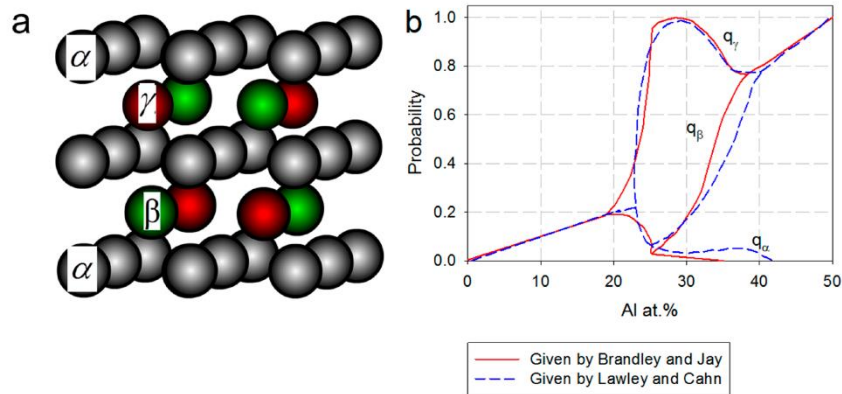


Fig. 2. Atomic arrangement in a B2 or D03 super-lattice; (b) Occupation probabilities of the lattice sites by Al in a Fe-Al system[2]

The B2 structure has the ideal stoichiometry of 50 at. % Fe-50 at. % Al and the D03 super structure has the ideal stoichiometry of 25 at. % Fe-75 at. % Al. However, the formation of lattice defects, such as vacancies or anti-sites, cause the large range of deviations from the stoichiometric composition.

2.1.2 Point defects and Dislocations

The type and concentration of the point defects in Fe-Al intermetallics can influence on the thermo-mechanical, magnetic and electrochemical properties. Moreover, the point defects affect the diffusion processes. It has been shown that vacancies could act as obstacles to dislocation movement. Additionally, strong interactions between structural defect and hydrogen could significantly influence the hydrogen concentration and penetration rates in iron aluminides and cause severe mechanical degradation [42].

Point defects have critical role in mechanical and chemical properties of intermetallics. Six various forms of point defects could exist on the D03(Fe_3Al) sublattices; Fe atoms on the γ sublattice (anti-

site Fe atoms), Al atoms on the α or β sublattices (anti-site Al atoms) and vacancies on the α , β and γ sublattices.

These defects let diffusion occur exclusively by nearest neighbor vacancy jumps, though diffusion occurs mostly via nearest neighbor jumps into vacant sites.

Slip direction in Fe₃Al in low temperature is $\langle 111 \rangle$. The difference between the active slip directions have significant influence on the ductility of intermetallics. Since the number of slip systems in the Fe-Al intermetallics is more than the required five independent slip systems, iron aluminides are intrinsically ductile. In Fe₃Al with D03 structure, a super lattice dislocation with a burgers vector of $\langle 111 \rangle$ is known to be dissociated into four super-partial dislocations, bound by two types of anti-phase boundaries (APBs) [43].

2.1.3 Mechanical Properties

One of the significant mechanical property of iron aluminides is their unusual increase in yield strength with increasing temperature up to 900 K [44] which is the basic reason to use them in high temperature conditions. It has been shown that Young's modulus of Fe-Al intermetallics with D03 super structure is minimum at room temperature. As it has been shown in **Fig. 3**, the Young's modulus increases with the enhancement of the Al content in each super lattice [45]. It shows the effect of aluminum on the strengthening of the interatomic bonds. Interestingly, the Young's modulus of aluminides with high Al content decreases significantly with the increase of temperature (about 40%).

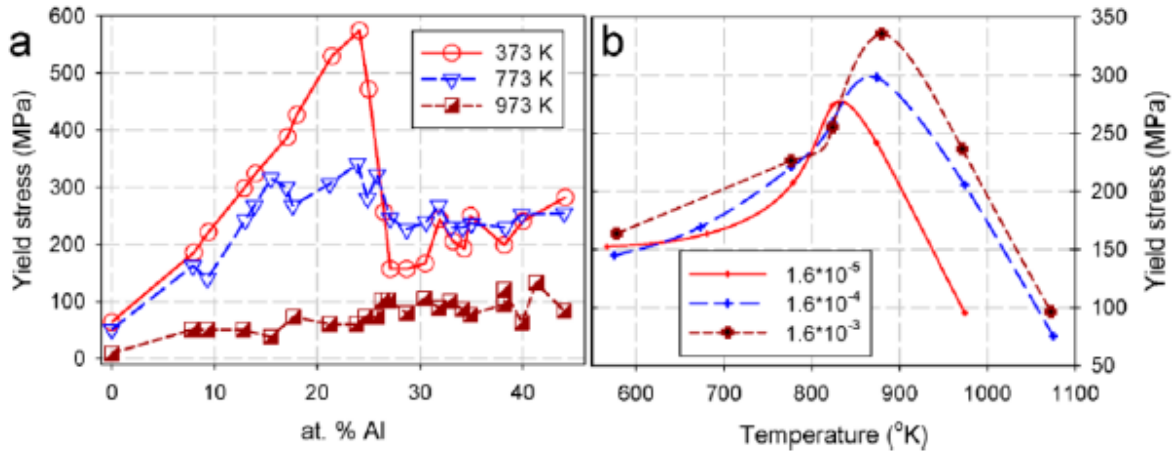


Fig. 3. (a)The influence of temperature and Al content on the yield stress of binary intermetallics (a)[45] ; (b)Stress anomaly and strain rate sensitivity of Fe–39.5 at. % Al intermetallics for a single slip system–oriented [44]

2.1.4 Alloying Elements

Several alloying elements add to the binary Fe-Al intermetallics to improve the mechanical, thermal or electrochemical properties. Some metallic elements such as Si, V, Cr, Mn, Co, Ni, Cu and Zn have great solid solubility and others such as Zr, Nb and Ta have restricted solid solubility in Fe-Al intermetallics. The β sublattice sites are preferred by Ti, W, V, Cr, Mo and Zr in a Fe_3Al super-structure[46].Cr is one of the most important alloying elements, and its input on various thermo-mechanical and electrochemical properties has already been studied extensively [1, 36, 47-49].

Palm studied an isothermal section for the Fe-Al-Cr system at 1000 °C [50]. He did not find any ternary intermetallic phases. It means the binary phases (Fe-Al) can dissolve considerable amounts of the third component (Cr) and the substitution does not make any changes in the crystallographic structure. The influence of Cr on ordering kinetics and dislocation configurations is not very significant [51].

2.1.5. Oxidation

In Iron aluminides oxidation, the formation of aluminum oxide is thermodynamically more possible than iron oxide since oxygen has a higher affinity to Al compared to Fe (the standard Gibbs energy of formation of $\alpha-Al_2O_3$ is -1,582,260 J/mol which is almost 6.5 times higher

compared to FeO). However, the experimental results performed on binary poly-crystals (with 15 and 40 at.% Al), oxidized at temperatures around 727 °C in synthetic air, show the existence of a thin Fe₂O₃, containing outer layer followed by an inner, nearly pure Al₂O₃ layer [2].

2.2. Electrochemical Nature of Corrosion

Corrosion of materials is the deterioration of a metal as a result of chemical reactions with its environment or flow of electricity during an electrochemical reaction in an aggressive medium [52].

In order to achieve a better understanding of the electrochemical nature of corrosion and the behaviour of metal in a corrosive environment, it is necessary to discuss the electrochemical aspects of the electrochemical reactions.

2.2.1. Electrochemical Reactions

Electrochemical reactions in the corrosion process consist of two half-cell reactions; the oxidation reaction, (equation 1), which takes place at the anodic sites and the reduction reaction, which occurs at the cathodic sites (equation 2). The oxidation and reduction could occur at separate locations on the metal. Alternatively, the location of anodes and cathodes can fluctuate randomly across the sample surface. The former case results in a localized form of corrosion, such as pitting, crevice corrosion, intergranular corrosion, or galvanic corrosion, and the latter case results in nominally uniform corrosion.

If a metal, M, for example with a valence number of +2, undergoes a corrosion process, the half-cell reactions can be written as:



The cathodic corrosion reactions in aqueous media could be one of two primary cathodic reactions. The hydrogen evolution reaction in acidic media :



And in neutral or basic solutions:



Each of the half reactions (1) and (2) or (3) will be in equilibrium at a specific potential called the reversible potential, E_{rev} . When all reactants and products are in their standard states with the activity of unity, the potential reaches a special value of reversible potential called the standard potential, E_0 . The electromotive force series is a list of half reactions that have been ordered by their standard potentials and indicates the tendency of one metal or ion to reduce the ions of any other metal below it in the series.

During corrosion process, the electrons liberated by anodic reaction are consumed in the cathodic process. A corroding metal does not accumulate any charge. It, therefore, means that these two partial reactions of oxidation and reduction must proceed simultaneously and at the same rate to maintain this electroneutrality[53]. The rates of the anodic and cathodic reactions must be equivalent according to Faraday's Laws. The total flow of electrons from anodes to cathodes which is called the "corrosion current," I_{corr} . Since the corrosion current must also flow through the electrolyte by ionic conduction, the conductivity of the electrolyte will influence the current. The anodic reaction usually is a metal dissolution, and the cathodic reaction is reduction of hydrogen ions.

2.2.2. Electrochemical Thermodynamics and Electrode Potential

The driving force for a fellow of electron between cathode and anode is a negative free energy change (ΔG). For electrochemical reactions, the free energy change is calculated from:

$$\Delta G = -n FE \quad (4)$$

Where n is the number of electrons, F is Faraday's constant, and E is the cell potential. Therefore, for a given reaction to take place, the cell potential is taken as the difference between the two half-cell reactions. The reason for the existence of such potential differences is the difference in the tendency of the anode and cathode towards continuing the reaction.

Another thermodynamic factor, which has a significant effect on corrosion reactions, is the factor of concentration. The equilibrium conditions require the same level of chemical activity for the

products and reactants. The change in energy activity due to a change in concentration of reactants and products can be then calculated using equation 4, which is also known as the Nernst equation:

$$\Delta G - \Delta G^\circ = RT \ln \frac{\text{activities of products}}{\text{activities of reactants}} \quad (5)$$

Where ΔG is the Gibbs energy, ΔG° is the Gibbs energy at standard condition, R is the gas constant, T is absolute temperature. Now by simplifying Equation 4 and Equation 5 the cell potential can be calculated (Equation 6):

$$E = E^\circ - \frac{RT}{nF} \ln \frac{\text{activities of products}}{\text{activities of reactants}} \quad (6)$$

Where E is the cell potential, E° is the electromotive force in standard conditions, while activities are the effective concentrations of the reactants and products that is calculated via the following formula:

$$a = \gamma \cdot c \quad (7)$$

Where c is the real concentration and γ is the activity coefficient. The activity coefficient of solids, electrons, and of species whose concentration does not change, e.g., solvents such as water, is equal to 1. For gases, partial pressure values are used in the place of activity coefficients, and the RT/nF is then converted to 0.0592 L.atm/mol.K at standard conditions. The direction of the reaction can be determined by the conventional assumption that the more negative cell potential always precedes through oxidation and the more positive half-cell will go through reduction [36].

2.2.3. Electrochemical Kinetics of Corrosion

The driving force of an electrochemical process is the potential difference between the cathode and anode. Although, the potential of cathode and anode potentials are equalized when both electrodes are connected and a current passes through the cell, resulting in the same potential of E_c and E_a at E_{corr} , which is a steady-state potential, where anodic current density is equal to cathodic current density, leading to the same anodic and cathodic reaction rates. That steady-state potential (E_{corr}) is called corrosion potential, and the corresponding current is called the corrosion current (i_{corr}).

2.2.4. Polarization

Despite equilibrium potential providing useful information about how the corrosion reaction is progressing, it cannot provide any data about reaction rate and kinetics. To measure the corrosion rate, usually an external current is applied, and the change in the electrode potential is measured. Polarization is the change in electrode potential due to this externally applied current, and the polarization value is the difference between the equilibrium potential and the potential measured under the externally applied current.

$$\varepsilon_a = E - E_{corr} \quad (8)$$

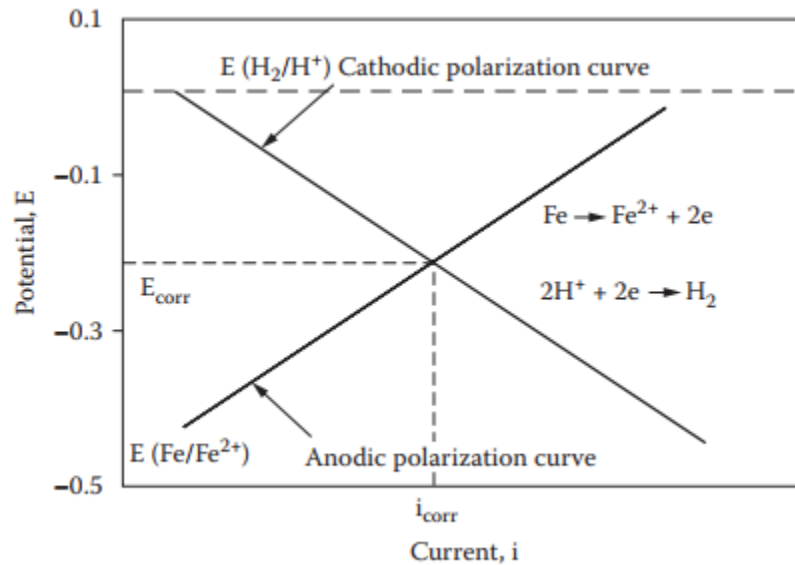


Fig. 4. The polarization of iron in acid[53]

Information about polarization effects gives an idea about which reactions take place at the electrodes. There are several types of polarization.

Activation Polarization: Activation polarization occurs because of a slow step in the electrode reaction. In such reactions, the activation energy in the form of an increase in potential is required for the reaction to proceed. This is best illustrated by the hydrogen evolution reaction. The hydrogen evolution reaction consists of several steps; the formation of hydrogen molecules is assumed the slowest step in the reaction sequence, and the rate of overall reaction will depend on

how fast or slow it proceeds. Therefore, to have a higher rate of reaction, expressed in terms of increased current density, an increase in potential should be applied [54].

Concentration Polarization: Concentration polarization occurs due to the concentration changes around the electrode with time. When current passes through the corrosion cell, some ions are consumed, and their concentrations are reduced, leading to an increase in the electrode potential. Consumed ions must be replaced with new ions from the electrolyte, but this process is limited with diffusion rate. Some factors such as increasing velocity, increasing temperature, and increasing concentrations will decrease the concentration polarization.

Ohmic Polarization: Ohmic polarization is due to the resistance in the circuit, which is also called IR ohmic overpotential reduction. Ohmic polarization is directly proportional to the current intensity between the anodic and cathodic sites of a corrosion process. If the current is stopped, then a reduction in the potential amount of IR also disappears simultaneously, while other polarization effects decrease slowly [37]. For many corrosion situations, these sites are adjacent to each other, and the ohmic drop is negligible.

2.2.4.1. Polarization Curves

Any electrode immersed in an environment will naturally have a potential, called the corrosion potential. At the corrosion potential the sum of all of the oxidation currents must equal the sum of all of the reduction currents:

$$\sum I_c + \sum I_a = 0 \tag{9}$$

Note that reduction currents (I_c) are negative. The corrosion potential is also called the open-circuit potential, free potential, or rest potential. The corrosion potential is a mixed potential indicating that its value depends on the rate of the anodic as well as the cathodic reactions. Furthermore, if the corrosion cell includes one anodic reaction and one cathodic reaction, the corrosion potential will be between the reversible potentials of the two half reactions [55].

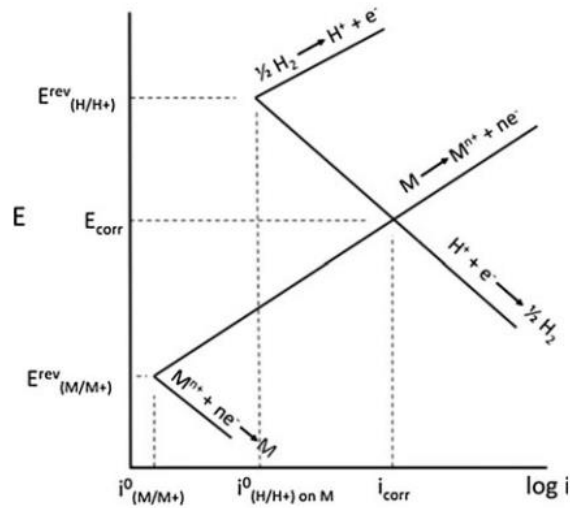


Fig. 5. Schematic Evans diagram for the corrosion of metal M by an acid showing the application of mixed potential theory[55]

In **Fig. 5**, $E^{\text{rev}}_{(M/M^{+})}$ and $E^{\text{rev}}_{(H/H^{+})}$ represent the reversible potentials for the metal M dissolution and hydrogen evolution reactions, respectively; $i^0_{(M/M^{+})}$ and $i^0_{(H/H^{+})}$ represent the exchange current densities for metal dissolution and hydrogen evolution on M, respectively.

Polarization curves of metals in solution can be determined by potentiodynamic polarization method. Using a potentiostat, a counter electrode, and a reference electrode, the potential of a sample is scanned in small increases over a range from usually about 250 mV below the corrosion potential to well above the corrosion potential. The potentiostat determines the current passed at the electrode surface as a function of the potential. The current density is easily calculated and is often plotted as a function of potential on a semi-log plot like that shown in **Fig. 6**. Such a plot is called a polarization curve.

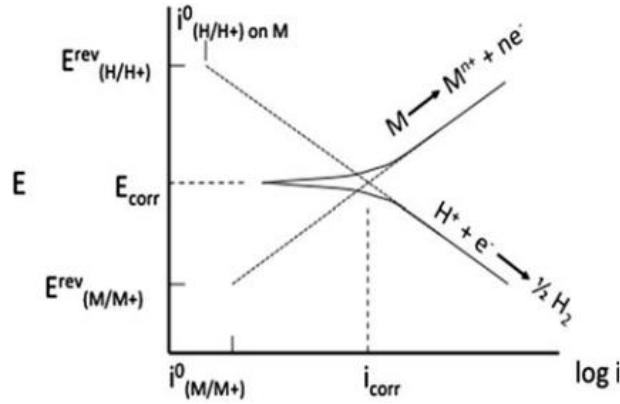


Fig. 6. Schematic measured polarization curve for metal M in an acid [56]

Note that the absolute value of current $\log i$ is plotted, as the log of a negative number is undefined. This plot presents the case of a metal corroding at a mixed potential in a solution containing an oxidizing agent. Far from the corrosion potential, both cathodic or anodic reaction rate increase and the related curve tends to follow the straight line illustrative of Tafel kinetics for the anodic reaction at high potentials and for the cathodic reaction at low potentials. At the corrosion potential (E_{corr}), $I_a = I_c$, so the measured or net current equals zero, the log of which is $-\infty$. Therefore in **Fig.6** the potential at which the curve points to the left (apparently approaches to $-\infty$) signifies the corrosion potential. Using the linear regions of the semilogarithmic plot and extrapolating to the corrosion potential, gives the corrosion rate (i_{corr}).

In a corroding system with a single anodic and a single cathodic reaction, such as illustrated in Fig. 6, the relationship of the current and potential is:

$$I_{\text{net}} = i_{\text{corr}} \exp \left[\frac{2.3(E - E_{\text{corr}})}{b_a} \right] - i_0 \exp \left[\frac{2.3(E - E_{\text{corr}})}{b_c} \right] \quad (10)$$

Where b_a and b_c are the anodic and cathodic Tafel slopes, respectively. This equation describes the net current when two different half reactions occur on a single electrode surface. The potentiostat manufacturer use equation (9) and Non-linear least squares fitting of the $i_{\text{net}}(E)$ by analysis software to provide values for the constants in the equation, i_{corr} , E_{corr} , b_a , and b_c [55].

2.2.4.2. Polarization Resistance

Polarization resistance (sometimes referred to as linear polarization resistance, LPR), is an electrochemical test method that measures the resistance of the specimen to oxidation in a corrosive environment while an external potential is applied to the system. Polarization resistance (R_p), can then be monitored, and directly related to the rate of corrosion [57].

In order to perform an experiment for monitoring the polarization resistance, an electrode needs to be polarized within the range 10 to 30 mV, relative to the corrosion potential at steady state, to ensure that active corrosion is occurring during the measurements. Then the polarization resistance can be specified by determining the slope of the linear region of the resulting curve at the corrosion potential. The relationship between change in potential and resulting polarization current R_p is given by equation 10:

$$\frac{\Delta E}{\Delta i} = R_p = \frac{\beta_a \beta_c}{2.3(i_{corr})(\beta_a + \beta_c)} \quad (11)$$

where i is the current density, i_{corr} is the corrosion current density, E is the applied voltage, and β_a and β_c are the anodic and cathodic Tafel slopes, respectively. It should be noted that equation 10 can be derived to calculate the i_{corr} . Once the corrosion current is known, the rate of corrosion can be determined from Equation 11:

$$corrosion\ rate\ (MPY) = \frac{0.13(i_{corr})EW}{A.d} \quad (12)$$

Where EW is the equivalent weight in g, A is the exposed area in cm^2 , d is the density of the specific test subject, and 0.13 is the metric time conversion factor. The rate of corrosion is measured in units of millimetre per year.

2.2.5. Active –Passive Behavior of Fe₃Al

Metals such as chromium, nickel, titanium, aluminum, magnesium, and iron that are above hydrogen in the electrochemical series, do not corrode in specific solution due to the oxide layers formed on their surfaces, resulting in passivity as observed in potential-pH diagrams. These metals automatically get passivated without the application of any external current under appropriate conditions. Auto-passivation occurs when the corrosion current (i_{corr}) is higher than the current needed to passivate the metal. Definition of passivity has been provided by the NACE/ASTM

Committee J01, Joint Committee on Corrosion “passive—the state of a metal surface characterized by low corrosion rates in a potential region that is strongly oxidizing for the metal”.

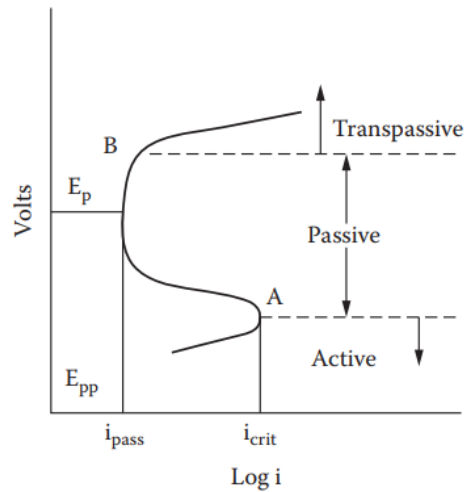


Fig. 7. The active-passive behaviour of a material

Active-passive behaviour is schematically represented by the anodic polarization curve in **Fig.7**. That describes the kinetics of passivity in a general way. Starting from lower potential, the curve starts out with a gradually increasing current as expected. However, at a critical point A (E_{crit}) there is a dramatic polarizing effect that drops the current to a point where corrosion is almost stopped (E_p). As this potential is increased further, there is little change in current flow until the next critical stage B; the current density starts to increase, resulting in either the initiation of pitting or entry into the transpassive region and the current again begins to rise [56].

Corrosion happens more rapidly in the active region and current increases with more positive applied potential. At point A, the corrosion rate increasing stops and the passivation begins. The potential at this point called passivation potential, E_{pp} and the corresponding value of current density referred as the critical current density. In the passive region, as the passivating film forms on the specimen, the current decrease rapidly. A small secondary pick in that small change in current is observed by increasing potential that determine the breaking of the passive film in transpassive region in which corrosion rate increases (point B).

Shankar Rao[1] in his review of the electrochemical corrosion behaviour of iron aluminides stated the aqueous corrosion behaviour of iron aluminides in both acidic and basic solution.

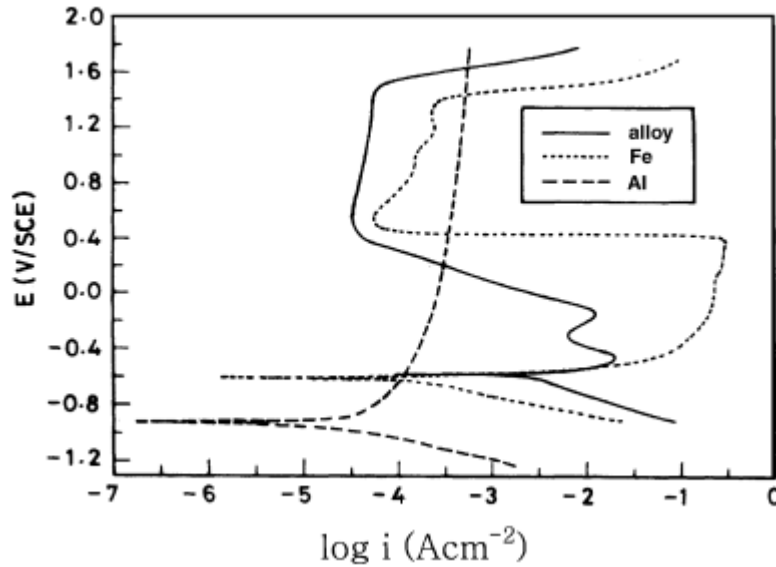


Fig. 8. Potentiodynamic polarisation curves of iron aluminide, pure Al and Fe obtained in 0.25 M H₂SO₄

Considering both Al and Fe polarization curve with Fe₃Al in 0.25M sulphuric acid (**Fig. 8**), the combined effect of Fe and Al has an advantage for iron aluminide over a wide potential range. At low potential, close to the corrosion potential of the aluminide, the spontaneous passivation tendency of Al helps to reduce active dissolution of iron aluminide by the formation of an Al₂O₃ film, while at the higher potential the presence of iron oxide makes an additional resistance to the passage of current with Al₂O₃. Therefore, the current density of iron aluminide in the passive region is lower than that of pure iron. In addition, the anodic critical current density ($i_{crit} \sim 20 \text{ mA cm}^{-2}$) of aluminide is more than its limiting current density for oxygen reduction (0.1 mA cm^{-2}), which makes the aluminide difficult to self-passivate in aerated conditions. The polarization curve of iron aluminide in the transpassive region seems to be similar to that of pure iron, and its transpassive potential is well above the equilibrium potential for oxygen evolution (0.96 VSCE for a measured pH of 0.6 and assuming the partial pressure of O₂ as 1 atm.).

2.2.5.1. Structure and chemistry of the passive film

Several studies were directed on passive film structure of iron aluminides with different Al contents in the alloy, different electrolytes, concentration and pH, and different formation

potentials [58-61]. Despite these variations among these studies they have some aspects in common that are as follow:

- An enrichment of Al in the form of Al (III) oxide/hydroxide on the surface during passivation. This enrichment is even more than the Al bulk concentration of the alloy.
- Al content in the passive film increases with increasing Al content in the alloy.
- Co-existence of iron and aluminum oxides on the surface during passivation
- Addition of alloying elements such as Cr and Mo facilitate the formation of their respective oxides (Cr_2O_3 and MoO_3) in the passive film along with Al_2O_3 .

Investigation of the passive layer by XPS spectra [58] illustrates that the outer part of the passive film mainly consists of mixed Al-Fe oxy-hydroxide whereas the inner part is of mostly an Al-rich oxide phase. In another study, elastic-ion scattering and XPS depth profiling [59] shows maximum enrichment of Al(III) within the centre of the passive film . The primarily formed Al(III)-rich film contains a large amount of hydroxide. However, during longer passivation time and at more positive potential the layer composition changes into a mixed oxide/hydroxide film with a larger amount of additionally formed iron oxide.

To get an idea about the mechanism behind the passivation behaviour of iron aluminides we take a look at the chemical reactions which take place after its immersion in the electrolyte. **Fig. 9** presents a schematic model for the passivation behaviour of iron aluminide. During the active dissolution of the alloy, whether it is FeAl or Fe_3Al , Iron atoms dissolve, and Fe ions enter to the solution. thermodynamically, Al_2O_3 has more negative free energy compared to iron oxide[59] and kinetically, the mobility of Al^{3+} is also low compared with iron ions within the barrier film[58]. Therefore, after active dissolution from iron aluminide, aluminum quickly converts into Al_2O_3 on the surface, whereas iron ions remain in the solution.

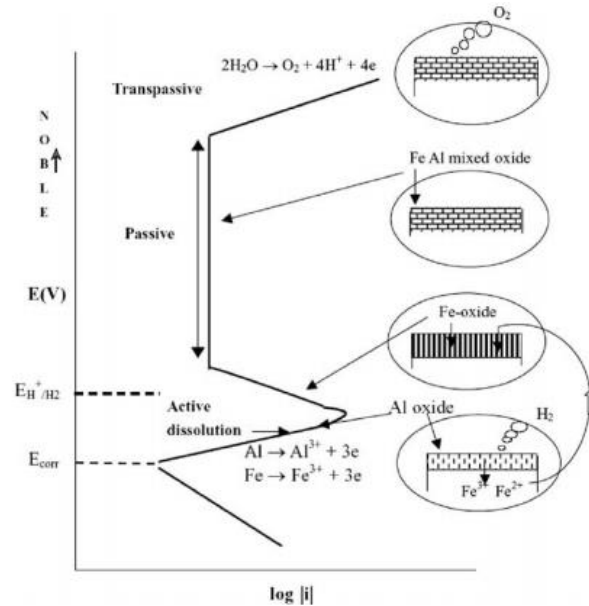


Fig. 9. Schematic model for passivation behaviour of iron aluminide in acidic electrolyte [1].

This Al_2O_3 layer is expected to have the role of a diffusion barrier similar to the case of pure Al for dissolution of iron from the surface. However, due to porosity in nature, it allows some iron to dissolve. By increasing the potential and from E_{crit} to pre-passive potential, FeO and Fe_2O_3 iron oxides start forming on the surface. It is assumed that the formation of these iron oxides on the surface of the passive film blocks the porosity of the Al_2O_3 passive film. In addition, the presence of iron oxides on the surface provides additional resistance to protectiveness of the passive film. Thus, a cooperative resistance of Al_2O_3 and Fe_2O_3 oxides drop the passive current density of iron aluminide to its minimum value in the passive region. As mentioned above with the shift of passive potential towards the noble direction more Al–OH starts forming. This can be explained by the following reaction:



Since the above-mentioned, oxides and hydroxide remains stable from their passive potential to the oxygen evolution potential for a given pH. Therefore, the transpassive region corresponds to the Oxygen evolution reaction [23].

2.2.5.2. Effect of aluminum content and chromium addition

Effect of aluminum content on the passivation behaviour of Fe-Al alloys in 0.1 N H_2SO_4 , studied by Chiang et al. [18]. Results show that Fe–Al alloys, exceeding 19 at %, have wide passivation

regions with low passivation current. In addition, when the Al content exceeds this range, the increment of Al content has a slight influence on passivation. In that work, the influence of Cr on passivation behaviour of alloys demonstrate that Fe-20Al-5Cr and Fe-30Al-5Cr have more stable passive film than those without Cr. These alloys, are likely to form a relatively more stable passive film with slight lower passivation current density at higher anodic potential. Consequently, the passivation behaviour of these alloys can be improved with Cr addition. Al tends to form a porous oxide film (separate oxide phase) in H₂SO₄ and Cr has the role of a strong oxide film-forming element by giving Fe–Al alloys, additional resistance to the passage of metal ions through Al oxide film. Therefore, it improves the passivation behavior by the formation of a film, composed of Cr(OH)₃ and Cr₂O₃ in alloys with higher Cr content [18].

In other work, Frangini et al. [62] conducted some experiments to determine the role of Cr in the passive film by incorporation from the solution rather than from the alloy. For this, Cr ions were incorporated into the passive film of FeAl from alkaline chromate solution through repetitive oxidation–reduction cycles and its corrosion behaviour was compared with Fe–(12–24)% Cr stainless steels in 0.5 M NaCl containing borate solutions. Their results revealed that the pitting potential of this alloy after treatment is comparable to those of stainless steels despite the fact that the Cr enrichment in the passive film of FeAl was not as high as in the passive film of the compared stainless steel.

Recently, Zamanzadeh and Barnoosh[48] made a detailed investigation on the electrochemical properties of Fe₃Al in a range of Cr concentration (0, 0.5, 4.0 and 5.0) while Al concentrations remained constant at the 26 at.% to gain a detailed understanding of effect of Cr on the electronic behaviour, thickness and effective capacitance of the passive layer. They revealed that Cr as an alloying element provides more resistance to pitting corrosion for passive film and decreases the average density of pits. However, addition of 5 at.% Cr to the binary Fe₃Al intermetallics does not prevent the pitting and crevice corrosion of alloys completely. They also stated that Cr³⁺ would substitute at the Al³⁺ site in the passive film because the Cr³⁺ size is 63 pm, slightly bigger than the size of the Al³⁺ ion (51 pm). During the formation of the passive film, Cr³⁺ diffuses into the solution/oxide interface. It can segregate at crystal imperfections sites cause of high energy defects and prevent chloride ions entering. Therefore, the entry sites may be blocked by the alloying

oxides. The saturation of the oxide/electrolyte could be seen by the changes of the flat-band potentials where no space charge arises in the passive layer [48].

2.3. Corrosion Measurement Techniques

The main purposes of corrosion testing, are generally evaluation and selection of materials for a specific application, evaluation and design of new alloys, determination of the aggressiveness of a medium, provide reference or database information; and study of the corrosion kinetics and mechanisms [63].

Corrosion laboratory tests can be defined into three categories [64]:

- Wetting of the surface by condensing media in a humid atmosphere (simulated atmosphere test)
- Spraying of aggressive medium (salt spray test)
- Immersion into corrosive liquid (immersion test)
- Electrochemical test

2.3.1. Electrochemical Methods

Electrochemical techniques are employed to identify the corrosion behaviour of many materials for many years. Since corrosion consists of electrochemical oxidation and reduction reactions, electrochemical measurements can provide valuable information relating to the factors that are needed to characterize the corrosion mechanism and rate.

The reactions that occur during a corrosion process create the corrosion potential. This potential should be measured regarding a reference such as a saturated calomel electrode (SCE). The potential difference between test specimen and the reference electrode is reported. The value of the potential (E) and current (I) or current density(i) can be specified by performing an electrochemical test.

Corrosion-related mechanisms, such as passivation and pitting, are slow processes and could be studied by applying ‘accelerating’ external potentials to the system. The curves of the applied

potential versus the specific current densities can be plotted for further quantitative interpretation and calculations.

The most frequently measurements are

1. Steady state corrosion potential (E_{corr})
2. Variation of E_{corr} with time
3. E- i correlation during polarization at constant current density(galvanostatic) and variable potential
4. E-i correlation during polarization at constant current potential(potentiostatic) and variable current
5. Electrochemical impedance under alternating potential conditions as a function of frequency
6. Electrochemical noise: fluctuations of the free potential or fluctuations of the current when a constant potential is maintained [64].

Frequently used electrochemical techniques in corrosion testing that can aid in identifying the corrosion processes of composite materials are open circuit potential, potentiodynamic polarization, cyclic polarization, and electrochemical impedance spectroscopy.

2.3.1.1. Open circuit Potential

Open circuit potential (OCP) can be considered as the simplest technique among the others. When it is employed in short-term (one hour or less), it usually is followed by the other methods. Furthermore, when it performed in long-term (one day or more), it can be considered as an individual test method to determine the electrochemical equilibrium of an electrochemical system by the time. The potential difference between the working and reference electrode is measured until a steady state is achieved. This final value is known as the corrosion potential (E_{corr}).

The variation of OCP of metallic materials as a function of time gives valuable information about film formation and passivation. A rise of potential in the positive direction indicates the formation of a passive film, a steady potential indicates the presence of an intact and protective film, and a drop of potential in the negative direction indicates breakage or dissolution of the film, or no film

formation[65]. **Fig. 10** is an example of OCP curves that is obtained from Al–TiC composites sintered at different temperatures in 3.5%NaCl solution for 1 h [66].

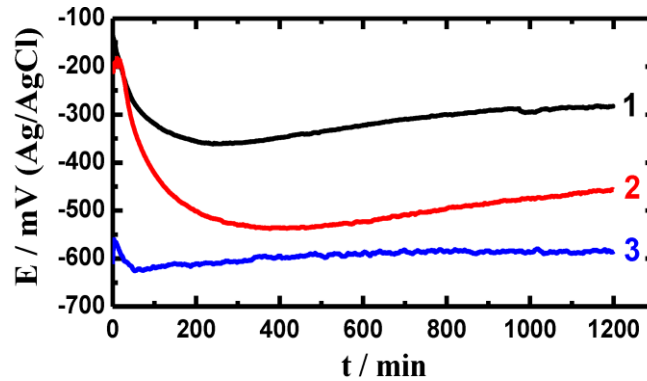


Fig. 10. Change of the open circuit potential versus time curves obtained for the Al–TiC composite sintered at (1) 900, (2) 1100, and (3) 1300 °C in 3.5% NaCl solution [65]

2.3.1.2. Potentiodynamic Polarization

Potentiodynamic polarization test illustrates the polarization characteristics of active material in the corrosive environment by plotting the current response as a function of the electrode potential. In this technique, potential scans from negative to positive and the resultant net current is measured. A complete current–potential profile can be plotted in a matter of a few minutes to a few hours, depending on the voltage scan rate. After a specific duration that the specimen

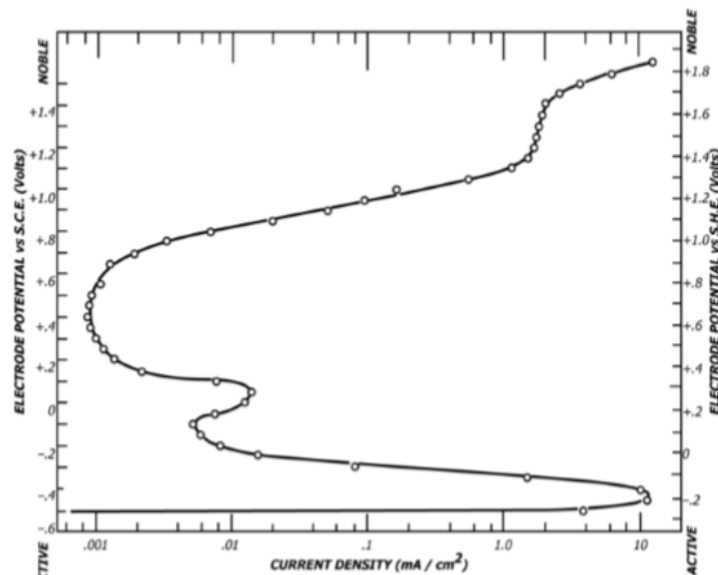


Fig. 11. Typical Potentiostatic Anodic Polarization Plot for Type 430 Stainless Steel in 1.0 N H₂SO₄[57]

immersed in corrosive liquid, it reaches a steady state condition and potential approaches to E_{corr} . The external voltage source used to force it to a potential slightly more positive than E_{corr} , the cathodic current becomes negligible with respect to the anodic component, and cathodic reaction occurs on the counter electrode surface. By increasing the potential, the polarization characteristics of a sample in special solution can be identified.

Important information, such as the ability of the material towards immediate passivation in a particular medium, and the specific potential at which this occurs, can be obtained from the potentiodynamic polarization curve. Such plots are also extensively used to predict the rate of corrosion in the passive region. **Fig. 11** is an example of potentiodynamic anodic polarization curve for 430 stainless steel [67].

2.3.1.3. Cyclic Polarization

Cyclic polarization is a type of the potentiodynamic polarization technique which is performed in a cyclic manner. Cyclic polarization is widely used to determine the tendency of specific materials towards pitting corrosion. It provides information on both corrosion characteristics and corrosion mechanisms.

The potential is scanned in a single cycle, and the size and direction of the hysteresis are examined to investigating pitting occurrence. The existence of the hysteresis is usually revealing of pitting, while the size of the loop is often related to the amount of pitting.

In the cyclic polarization test, first, the OCP is scanned, and the test starts at the corrosion potential. The potential then is increased in a positive direction up to the point a specific current density is reached (set by the user). Once the maximum current density is reached, the experiment is programmed to change the potential in the opposite direction [68].

The reversed potential traces a hysteresis loop, which may close at the protection or passivation potential. If the passivation and the corrosion potential have the same value, or the protection potential is more negative, the likelihood of pit formation becomes higher [69]. This method can also be used for predicting the occurrence crevice corrosion.

Fig. 12 shows a typical cyclic polarization plot. The E_{corr} , E_b and E_p parameters are represented the corrosion potential, passivation breakdown potential and protection potential respectively.

When $E_p > E_{corr}$ As displayed in **Fig. 12**, the repassivation is more likely, and In case of $E_p < E_{corr}$ sample remains in an active state and pitting increases continuously [70].

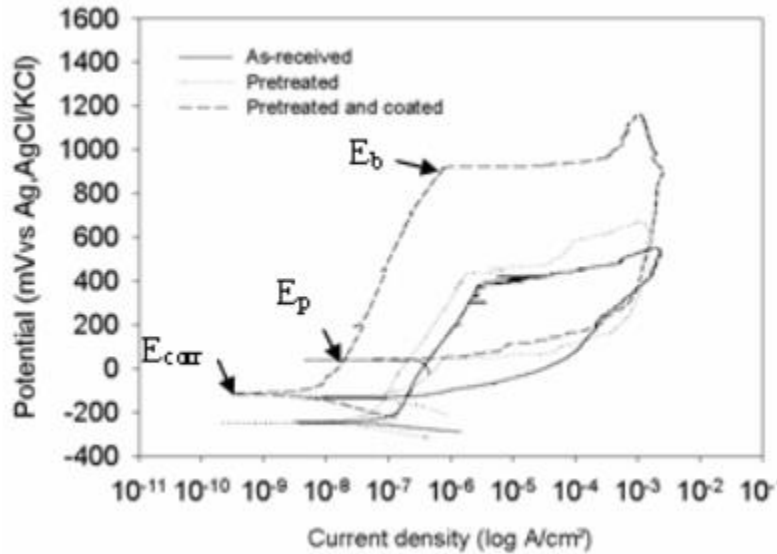


Fig. 12. Typical Cyclic polarization curve [70]

Additionally, the size and shape of the cyclic polarization loop can be a parameter to interpret the results. For example, if the reverse current has a higher value than the current in the forward direction, the formation of a larger hysteresis loop will demonstrate a higher tendency of the material to form pits [71].

2.3.1.4. Electrochemical Impedance Spectroscopy

Impedance measurements are employed to achieve corrosion rate and reaction mechanisms of the process at corroding surface [64]. Impedance just like resistance represents a barrier to the flow of electrons or current. In direct current, only resistors produce this effect while for AC circuits, two other circuit elements, capacitors and inductors, impede the flow of electrons. The effect of capacitors and inductors is given the name reactance, symbolized by X and measured in ohms (X_C for capacitive reactance and X_L for inductive reactance). The circuit elements in impedance and their equation is described in Table 1 [63].

For DC signal according to Ohm's law, $V = IR$, where V is the voltage across a resistor in volts, R is the resistance in ohms, and I is the current in amperes. For AC signals, $E = IZ$, where E and I are waveform amplitudes for potential and current, respectively, and Z is the impedance.

The impedance of a system at a given frequency is defined by two terms which relate the output current, the input voltage.

In a specific system with AC signal, the voltage is a function of time

$$E = E_0 \sin(\omega t) \quad (14)$$

Where E_0 is the amplitude of the signal and ω is the angular frequency ($2\pi f$) and, t is time in second the current is also function of time

$$I = I_0 \sin(\omega t + \varphi) \quad (15)$$

Where I_0 is the amplitude of the current and φ is the phase angle. The ratio of voltage amplitude to that of the current defines the impedance term


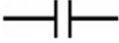

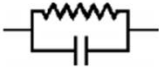
$$|Z| = E_0 / I_0 \quad (16)$$

To calculate the impedance of the system:

$$Z = \frac{E}{I}$$

$$Z = \frac{E}{I} = \frac{E_0 \sin(\omega t)}{I_0 \sin(\omega t + \varphi)} = Z_0 \frac{\sin(\omega t)}{\sin(\omega t + \varphi)} \quad (17)$$

Table 1. Circuit elements in impedance and their equation[63]

Circuit element	Impedance equation
	$Z = R + 0j \quad j = \sqrt{-1}$
	$Z = 0 - j/\omega C \quad \omega = 2\pi f$
	$Z = 0 + j\omega L \quad \omega = 2\pi f$
	$Z = \frac{R}{1 + \omega^2 C^2 R^2} - \frac{j\omega CR^2}{1 + \omega^2 C^2 R^2}$

EIS method is a beneficial method to study the electrochemical reaction states. The impedance measurement employed to determine the electronic components. **Fig. 13(a)** shows the model of the interface proposed by Helmholtz. In a simple case, the interface can be modeled by an equivalent circuit as shown in **Fig. 13(b)**. This is also called a Randles circuit, which is made of a double-layer capacitor in parallel with a polarization resistor. This is also called a Randles circuit, which is made of a double-layer capacitor in parallel with a polarization resistor (or charge-transfer resistor, R_{ct} ,) and Warburg impedance, Z_w , connected in series with a resistor that measures the resistance of the electrolyte, R_s .

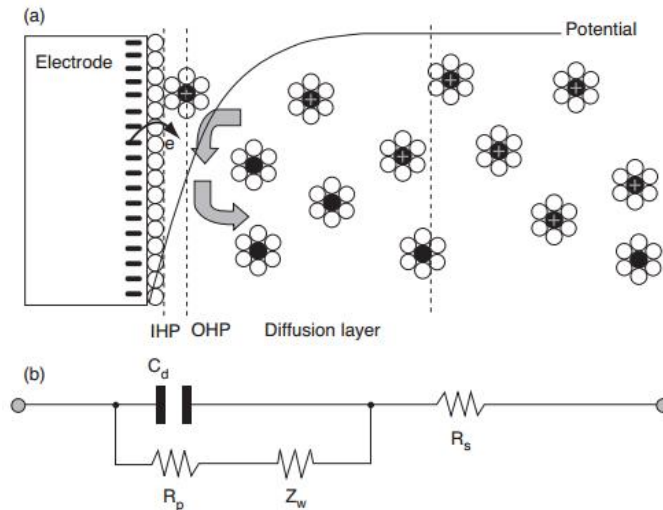


Fig. 13. A simple metal–aqueous solution interface in which the vertical dotted lines in (a) can match the electronic components determined after EIS studies [63]

In order to obtain an Impedance plot, the EIS data are recorded as a function of the frequency of an applied AC signal at a fixed working point of the polarization curve. In corrosion studies, this working point is often E_{corr} . The EIS measurements results are a set of amplitude and phase values for a range of frequencies; these can be presented in two ways: Bode plot and Nyquist plot.

The bode plot presents a log of frequency in x axis and both the absolute value of the impedance and phase shift on the y axis. **Fig. 14** presents a Bode plot for the equivalent circuit of Randles equivalent circuit [64].

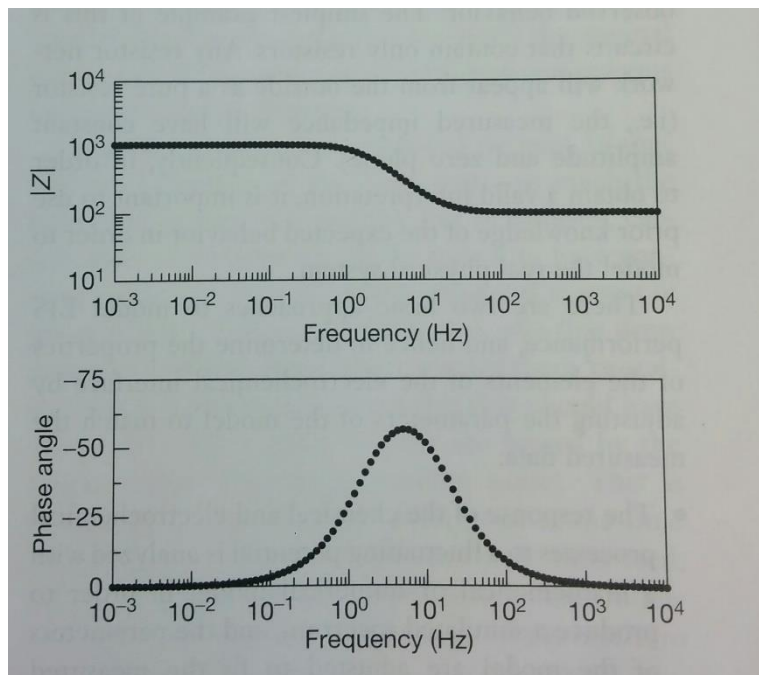


Fig. 14. Example Bode plot for the equivalent circuit of Randle's circuit[72]

The Nyquist diagram normally plots the imaginary part (Z'') of the impedance versus real part (Z'). It is also known as cole-cole plot or a complex impedance plane plot. Since the majority of the responses of corroding metals have negative Z'' , it is conventional, for corrosion studies, to the plot $-Z''$ against Z' . In this plot the y axis is negative, and each point on the Nyquist plot is the impedance at one frequency. **Fig. 15** shows an Equivalent electrical circuit model for a simple corroding electrode (left) and related Nyquist plot.

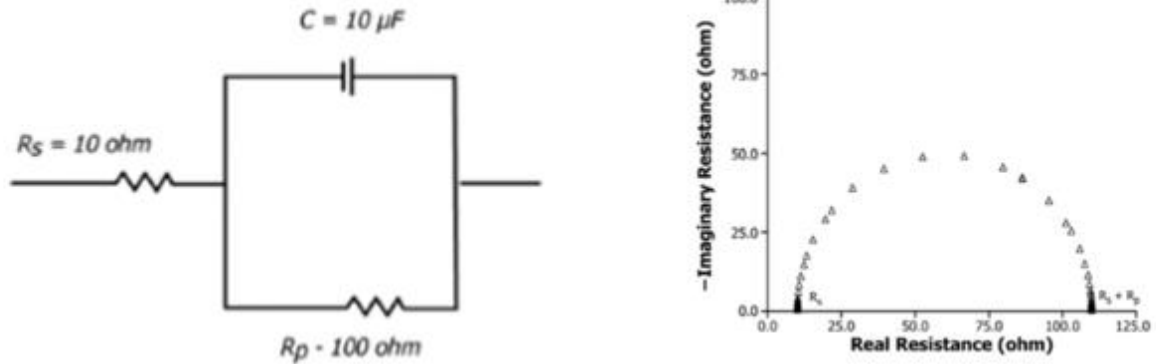


Fig. 15. Equivalent electrical circuit model for a simple corroding electrode (left) and related Nyquist plot for the equivalent circuit (right) [72]

In practical, the measured impedance spectra may differ from ideal or theoretical behaviour. The loops (or time constants) do not show a perfect semi-circle shape in Nyquist representation. This non-ideal behaviour may arise from coating heterogeneities as roughness, inhomogeneous composition etc. In such a case the coating cannot be described by a simple capacitor. This one is generally replaced by a constant phase element (CPE) whose impedance is given by

$$CPE = Y_0 (j\omega)^n$$

n accounts for non-ideal behaviours: when it equals to 1, the CPE is a pure capacitance and when it equals zero, the CPE is a pure resistance[73].

Depending on the system studied, there can be two or more such parallel RCs (resistance and capacitances) in the fitted circuit. Then the number of time constants is number of parallel RC or R and CPE components that can be visually estimated from the number of semicircles in the Nyquist plots.

2.3.2. Microstructural Analyses

The microstructural analysis is extensively performed to evaluate the surface of samples. Methods such as scanning electron microscopy (SEM), energy dispersive X-ray spectroscopy (EDS) and X-ray diffraction (XRD) confirms important information such as the grain size, distribution of

chemical elements within the structure, and the formation of possible phases due to the chemical corrosion reactions.

While SEM is known as one of the more useful techniques to study the effects of corrosion on microstructures of many materials, XRD is widely used for crystalline phase analyses of the starting powders, densified cermet and coatings, and potentially any corrosion induced oxides formed on the surface.

2.3.3. Chemical Analyses

X-ray photoelectron spectroscopy (XPS) techniques used to analysis of passive films formation for metals and alloys from 1970's. However, this technique usually faces such problems as (a) very high surface coverage of oxygen resulting from the layers of bound water and hydroxyl groups and the chemical effects of in vacuum dehydration and(b) oxidation of surface ions to higher states during transport to the analysis chamber [73].

Schaepers and Strehblow made a wide investigation on passive layers of Fe-Al alloys with XPS and elastic-ion scattering spectroscopy (ISS) under inert conditions on sputter-cleaned. In that work, the aluminum content was 8, 15 and 22 at%, which meets the homogeneity region of α -Fe in the Fe-Al phase diagram. X-ray photoelectron spectroscopy (XPS) studies revealed an accumulation of aluminum oxide within the centre of the passive layer, which is confirmed by ISS and XPS depth profiles. Angular-resolved XPS measurements suggest a continuous structural change of the chemical film during its growth [74].

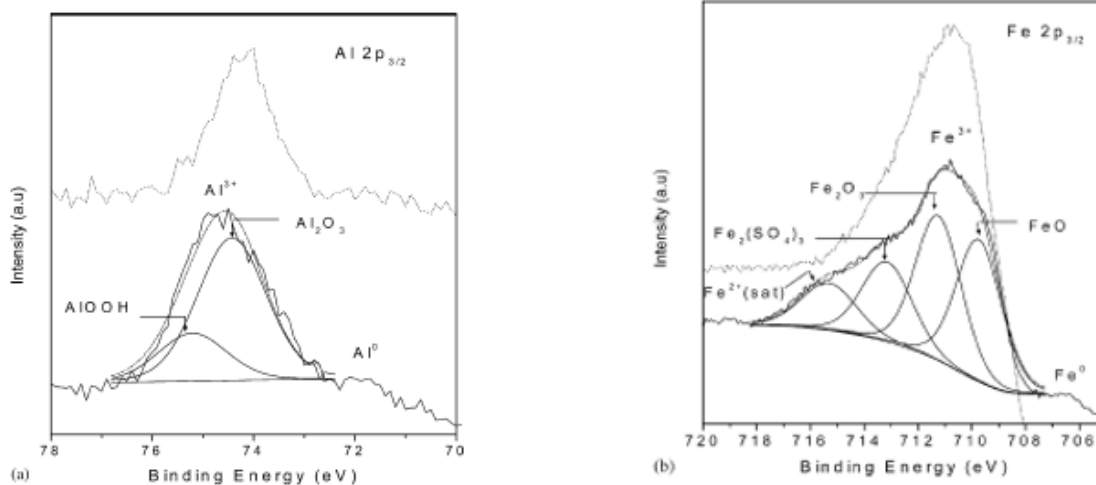


Fig. 16. XPS spectra for (a) Al and (b) Fe spectra for thermally oxidized elements at 800 °C (dotted lines) and passivated elements in 0.25 M H₂SO₄ at 1 VSCE. [1]

Some Authors compared the chemistry of passive films with that of the air-oxidized films in order to differentiate film properties in wet and dry conditions by XPS [58, 75]. In such study, XPS spectra of the iron aluminide exposed to the 0.25 M H₂SO₄ solution at 1 V_{SCE} and iron aluminide oxidized in the O₂ atmosphere at 800 °C for 10 min are compared (**Fig. 16**). Notably, in the case of the passivated sample, there is a shift in the Al³⁺ peak towards high BE, it revealed coexistence of Al³⁺ as Al₂O₃ and Al-OH at 74.49 and 75.29 eV, respectively. In **Fig. 16(b)**, the peaks of iron at 711 eV corresponding to Fe³⁺. Passive spectra reveal multiple peaks assigned to oxides and sulphates. Contrasting in the case of Al, there is no difference in the peak position of Fe³⁺ between the oxidized and passivated samples. This demonstrates that Al exists in the form of an oxide and hydroxide while Fe exists in the passive film only as an oxide.

In another work [59], investigation of the passive layer by XPS depth profiling illustrated that maximum enrichment of Al(III) within the centre of the passive film. The initially formed Al (III)-rich film contains a large amount of hydroxide. However, like any other passivating alloy during longer passivation time and at more positive potential the layer composition changes into a mixed oxide/hydroxide film with a larger amount of additionally formed iron oxide.

2.4. HVOF Thermal Spray Coatings

Thermal spraying is a well-known technology for applying wear and corrosion resistant coatings in many industrial sectors, such as aerospace, automotive, power generation, petrochemical and offshore and recently in biomedical, dielectric and electronic-coatings.

In thermal Spraying, fine molten particles impinge on the substrate surface and form a coating. A coating of the order of 20 microns to several millimetres can be formed using thermal spraying depending upon the methods and feed rate. The quality of the coatings is evaluated by the phase stability, coating density, adhesive strength, hardness, toughness, oxide contents and surface roughness. Thermal Spray is used for a group of processes in which metallic, ceramic, cermet and some polymeric materials in the form of powder, wire, or rod are fed to a torch or gun with which they are heated to near or somewhat above their melting point. Plasma spray, electric arc wire spray flame spray, high velocity oxy-fuel spray (HVOF) are the most popular of thermal spraying techniques.

In the early 1980s, Browning and Witfield introduced a unique method of spraying metal powders, called High-Velocity Oxy-Fuel (HVOF). The process utilizes a combination of oxygen with various fuel gases including hydrogen, propane, propylene, hydrogen and even kerosene.

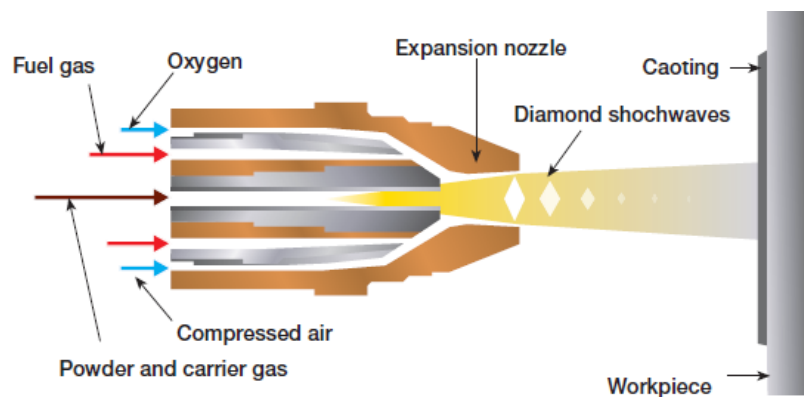


Fig. 17. Schematic diagram of the high-velocity oxy-fuel spray process (HVOF) [76]

In the HVOF process, fuel and oxygen are entered into the combustion chamber together, and the spray powder comes through from other side (**Fig. 17**). The combustion of the gases provides the

temperature and pressure needed to flow of the gases through the nozzle. The flame temperature is in the range of 2500 °C to 3200 °C. Therefore, the powder particles partially or completely melt during the flight through the nozzle [77].

The ability to produce dense coatings with a low amount of degradation, oxidation of metallic materials, and phase transformations is the main benefits of the HVOF process. This is due to the short dwell time of the particles in a relatively cold flame. It is widely used to produce cermet and metal coatings [77].

2.5. Summary

Intermetallic matrix composites were an interest owing to the combination of high specific modulus, strength, and wear resistance. Fe₃Al as a matrix has the superior properties and its relatively low wear resistance can also be improved by the addition of cermet as reinforcement phase. TiC has been found to be a suitable choice to reinforce the Fe₃Al matrix due to high hardness and high-temperature stability with the iron aluminide matrix [4].

In metallurgy and materials department of Laval University, a detailed project concerning the Fe₃Al matrix composites coatings that produced by HVOF techniques is defined for an industrial application. This project includes different methods of powder production and investigation of their mechanical and electrochemical properties. Mahdi Amiriyani as a Ph.D. candidate, in his work, studied the dry sliding wear behaviour of Fe₃Al/TiB₂ [78] and Fe₃Al/TiC composites provided by HVOF in which, the coating powder feedstock, was produced by high-energy ball milling of Fe₃Al, Ti and graphite powders. He also investigated the effect of TiC addition on dry sliding wear rates of the coatings at sliding speeds ranging from 0.04 to 0.8 m s⁻¹ and under a constant load of 5 N. The composite coatings with 0,10,30,50 and 70 mol.% TiC was evaluated and the results revealed that the Vickers hardness and wear resistance of the coatings increased with increasing TiC content in the Fe₃Al matrix. He has studied the wear mechanism and showed that the mechanism strongly depends on the sliding speed and the content of TiC particles. It was observed that at low sliding speed, the predominant wear mechanism of the coatings with 0, 10 and 30 mol.% TiC was fatigue wear, whereas, at high sliding speeds, the wear mechanism is oxidation. For Fe₃Al–50 mol.% TiC and Fe₃Al–70 mol.% TiC composites, abrasive and oxidation wear are most likely the dominant wear mechanisms[4]. He also compared the phase composition,

microstructure, microhardness and elastic modulus of unreinforced Fe₃Al and Fe₃Al/TiC composite coatings reinforced with 30 and 50 vol.% TiC particles [26].

In other work, Hadi Ghazanfari, as a Ph.D. candidate at Laval University, used combustion synthesis of pure elemental powder of Fe, Ti, Al and C to provide HVOF feedstock powder. In this method, the powders were mixed and pressed under 200 MPa pressure and placed in a preheated furnace at 1100 °C to ensure the highest possible heating rate. He likewise investigated the effect of TiC particles on the wear resistance of Fe₃Al/TiC composite coatings at sliding speeds ranging from 0.04 to 0.8 m.s⁻¹ and under a constant load of 5 N and revealed that the coatings in which feedstocks powders prepared by combustion synthesis exhibit 2 to 20 times higher wear resistance than the coatings with powder that prepared by ball milling. The best performance was related to a coating containing 70 mol.% TiC at highest speed.

CHAPTER 2

EXPERIMENTAL

3.1. Composite Coatings Fabrication

In this work, the samples were two reinforced composite coatings of $\text{Fe}_3\text{Al}/\text{TiC}$ and $\text{Fe}_3\text{Al-Cr}/\text{TiC}$ and Fe_3Al . These samples were applied on mild steel plates as a substrate using HVOF technique. In HVOF processing the feedstock powder were prepared by mechanical alloying of commercial iron aluminide (Fe_3Al , 96 % pure, Ametek), titanium (Ti, 99.4 % pure, Alfa Aesar), graphite (C, 96 % pure, Asbury Graphite Mills) and chromium (Cr, 99 % pure, Alfa Aesar). The nominal composition of each sample is given in **Table 2**.

Table 2. Nominal Composition of samples

Sample	at.% of elements				
	Fe	Al	Ti	C	Cr
Fe_3Al	75	25	0	0	0
$\text{Fe}_3\text{Al}/\text{TiC}$	50	16.66	16.66	16.66	0
$\text{Fe}_3\text{Al-Cr}/\text{TiC}$	37.5	12.5	12.5	12.5	25

A high-energy ball mill (Zoz, GmbH, Simoloyer) were employed to mix the powder. A 300 g-batch of each powder mixture was milled under argon atmosphere for 6 hours. Hardened steel balls were used for milling while the ball to powder weight ratio was 10:1.



Fig. 18. High energy ball milling apparatus

The milled powders were then heat treated at 1000 °C for 2 hours under 106 mbar vacuum. After heat treatment, as it is indicated in other work [4], XRD patterns contain Fe_3Al and TiC peaks.

Heat treated powders utilized as feedstock of HVOF gun to make a composite coating on mild steel plates (AISI1020) with dimensions of 190 mm×120 mm×5 mm. the substrates were sand-blasted and then washed with acetone and ethanol in order to roughen and clean the surface prior to deposition. HVOF system was a PraxairJP-8000HVOF spray with spray parameters listed in **Table 3**. The substrates were sand-blasted and then washed with acetone and ethanol prior to applying the coating. The carrying gas was Argon and Kerosene used as the fuel during the HVOF deposition. 5-10 micron of coating applied in each pass.

Table 3. HVOF spraying Parameters

Oxygen flow rate (m ³ /s)	1.5×10^{-2}
Kerosene flow rate (m ³ /s)	5.57×10^{-6}
Carrying gas	Argon
Spraying distance (m)	0.38
Number of deposition passes	5



Fig. 19. HVOF gun that applied the coating

3.2. Preparing Samples for electrochemical tests

The coatings which have applied by HVOF used as samples for electrochemical evaluation. The surface was not polished in order to not reduce the thickness and evaluate the corrosion behaviour in the same condition as they are employed in the industry. Samples were rinsed with ethanol and dried before performing the experiments.

For electrochemical impedance spectroscopy experiments, samples were mounted in cold setting epoxy resin with one end soldered to the wire with solder paste. The surface area of 1 cm² of the coating was in contact with the solution. This electrode further cleaned with distilled water and rinsed with water and ethanol and further assembled in a three-electrode Teflon holder that was immersed in the solution.

3.3. Operating Parameters and Solutions

Operating parameters in all electrochemical evaluation were similar. Operating temperature was room temperature and no heating applied while conducting experiments, therefore, electrochemical measurements were performed at 22 ± 3 °C.

Stirring rate of 60 rpm was applied during electrochemical studies to make electron transfer easier and to remove the bubbles from the surface of the sample and to approach to the actual condition that coating is supposed to work in. Stirring rate was controlled using a magnetic agitator device.

In this work, two kinds of the electrolyte were used to perform electrochemical tests.

- 1- 3.5 wt.% NaCl solution in distilled water with sodium chloride salt (99 % pure NaCl)
- 2- 0.25 molar solution of Sulphuric acid.

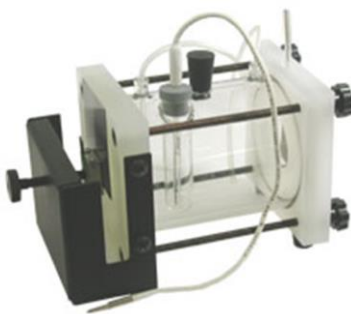


Fig. 20. K0235 Flat Cell used for OCP and polarization tests

A flat cell, K0235 model was employed for open circuit Potential (OCP), potentiodynamic polarization. This type of cell can accommodate any size and shape of samples without cutting. The volume of the cell contains 250ml of electrolyte (**Fig. 20**). An Ag/AgCl was used as a reference electrode and a platinum mesh as the counter electrode. All the potentials are subsequently reported

respect to Ag/AgCl electrode. These tests were carried out using a VersaSTAT3 Potentiostat-Galvanostat workstation equipped with VersaStudio software.



Fig. 21. VersaSTAT3 Potentiostat -Galvanostat workstation

Since Versa STAT 3 potentiostat-Galvanostat system was not equipped with electrochemical impedance spectroscopy test, electrochemical impedance spectroscopy (EIS) was conducted using potentiostat Gamry Reference 3000.

3.3. Experimental Procedures

3.3.1. Open Circuit Potential Test

The change of potential with time (OCP) curves was collected over 20 hours of immersion for Fe₃Al, Fe₃Al/TiC and Fe₃Al-Cr/TiC in solution. In this technique, it does not apply any voltage or current (Cell OFF), and simply measures the voltage difference between the working-sense and the reference electrodes. The collection of data started 5 minutes after immersion and rate of the scan was one point per second. The natural corrosion of coatings in 3.5 % NaCl solution investigated.

3.3.2. Potentiodynamic Polarization Studies

The solution of 3.5 wt.% NaCl was used during electrochemical tests. Prior to each polarization measurement, a minimum of 1 hours of sample immersion in the electrolyte was allowed to ensure nominally steady-state conditions. The potential scan rate was 1 mV/s. The applied potential was controlled during testing using the VersaStudio software. Potentiodynamic polarization measurements were conducted by scanning from -0.6 to +2 V (vs. OCP) for all coatings. Experiments have been repeated until three same results achieved. The ASTM standard method for potentiodynamic polarization resistance measurements and the subsequent calculation of corrosion rates (Equation 18) was followed[79, 80]

$$CR = \frac{i_{corr}}{\rho} EW \quad (18)$$

where CR is the rate of corrosion (given in mm/year), i_{corr} is the current density at the corrosion potential (in A/cm²), K is a constant (equal to 3.27×10^{-3} mm g/ μ A cm yr), ρ is the density (in g/cm³) and EW is the equivalent weight for the specific composition. Calculation of equivalent weight (EW) values for the alloys according to the standard practice of ASTM G102[67] and following equation.

$$EW = \frac{1}{\sum \frac{n_i f_i}{W_i}} \quad (19)$$

where:

f_i = the mass fraction of the i^{th} element in the alloy,

W_i = the atomic weight of the i^{th} element in the alloy, and

n_i = the valence of the i^{th} element of the alloy

3.3.3. Electrochemical Impedance Spectroscopy (EIS)

Electrochemical impedance spectroscopy (EIS) was conducted using potentiostat Gamry Reference 3000. The working electrode was the coated plate mounted in epoxy resin with a 1 cm² of surface area, and cathode was a platinum foil with a surface of 1 cm². Electrodes were rinsed with ethanol and dried before tests. The Ag/AgCl (KCl sat.) was used as reference electrode. Prior to electrochemical impedance spectroscopy, 1-hour stabilization time was considered then the frequency scanning was performed from 10⁻² to 10⁵ Hz with a root-mean-square potential amplitude of 5 mV. Experiments were repeated until three same results achieved.

3.3.4. Energy Dispersive Spectrometry (EDS)

In order to the analysis of the surface of coatings after performing the potentiodynamic polarization tests, a scanning electron microscope (SEM) JEOL JSM-840A, equipped with an energy dispersive X-ray spectroscopy (EDXS) was employed. Morphology and elemental analysis of the coating were done to evaluate the composition of corrosion products.

3.3.5. X-ray Photoelectron Spectroscopy (XPS)

Surface chemistry analysis was performed using an X-ray photoelectron spectroscopy (XPS). The ESCA spectrometer was an AXIS-ULTRA instrument by KRATOS (UK). X-ray source was a monochromatic Al K-alpha source operated at 300 watts. The analyzer is run in the constant pass energy mode, with the lens system in the "hybrid" configuration, i.e. with both the magnetic and the electrostatic lenses, and the electrostatic lens aperture in the "slot" position. This assures the

highest sensitivity with an analyzed spot approximately 700 microns x 300 microns, which is the size of the monochromated X-ray beam. Multichannel electron counting is performed with an 8 channel electron multiplier detector. The pressure during analysis is in the 10^{-8} Torr range while the base pressure is 5×10^{-10} Torr.

The electrostatic charge which appears on electrically insulating samples under X-ray irradiation was neutralized with the integrated very low energy electron flood gun, the parameters of which were set to optimize energy resolution and counting rate. The electron beam was normal to sample holder's bottom, and x-ray beam was at 30 degrees to it. Photoelectrons are collected along sample surface normal.

Elemental analysis was performed by recording survey spectra at a pass energy of 160eV and energy step of 1eV per channel. Apparent relative concentrations were calculated using the CasaXPS software with the appropriate sensitivity factors and are displayed on the survey spectra in atomic percent. Concentrations are named apparent because they are calculated under the hypothesis that the sample is homogeneous laterally and in depth over the analyzed area (approximately $800 \mu\text{m} \times 400 \mu\text{m} \times 5\text{-}10 \text{ nm}$). Concentrations thus obtained from XPS can be very different from bulk concentrations such as measured with EDS or WDS.

High-resolution spectra are recorded at pass energies of 40 and 20eV and step sizes of 0.1 and 0.05. Peak decompositions were performed using the same CasaXPS software. C1s spectra are usually recorded mainly for binding energy correction, because of the use of the neutralization gun which overcompensates the electrostatic charge; as usual aliphatic/contamination carbon component is set at 285 eV and the correction is propagated to all spectra of the same sample recorded in the same conditions.

3.3.5. Cyclic Polarization in sulphuric acid solution

The cyclic electrochemical analysis was performed in 0.25 M sulphuric acid solution, after one hour of stabilization. Polarising the surfaces carried out with an initial voltage of -0.5 V to +2.0 V, and then cycling back to 0.5 V as the final potential, with respect to the Ag/AgCl reference with a scanning rate of 0.166 mV/s.

CHAPTER 3

RESULTS AND DISCUSSION

4.1. Open circuit potential

The variation of open circuit potential (OCP) of metallic materials as a function of time provides valuable information about the formation and the nature of the oxide film and its capability of passivating the sample. The rise of the potential in the positive direction indicates the formation of a passive film, a steady-state potential indicates the presence of an intact and protective film, and a drop of the potential in the negative direction indicates breakage or dissolution of the film or the absence of film formation [65].

Fig. 22 illustrates the reproducible stabilization of the OCP for Fe_3Al , $\text{Fe}_3\text{Al}/\text{TiC}$ and $\text{Fe}_3\text{Al-Cr}/\text{TiC}$ coatings in freely aerated 3.5 % NaCl solution. For all coatings, during stabilization that takes place at the early moments of immersion, the potential rapidly shifts towards the negative potentials. This behaviour is most likely due to the dissolution of the existing oxide layer, formed on the sample before immersion. The potential is then stabilized, and no change is observed until the end of the experiment over a time period of 20 hours. This indicates that an equilibrium is established between the corrosion and the formation of an oxide film on the surface. $\text{Fe}_3\text{Al}/\text{TiC}$ and $\text{Fe}_3\text{Al-Cr}/\text{TiC}$ coatings reaching an OCP value between -440 and -480 mV and exhibited lower corrosion potential compared to Fe_3Al coating with stabilizing potential at -580 mV vs reference electrode.

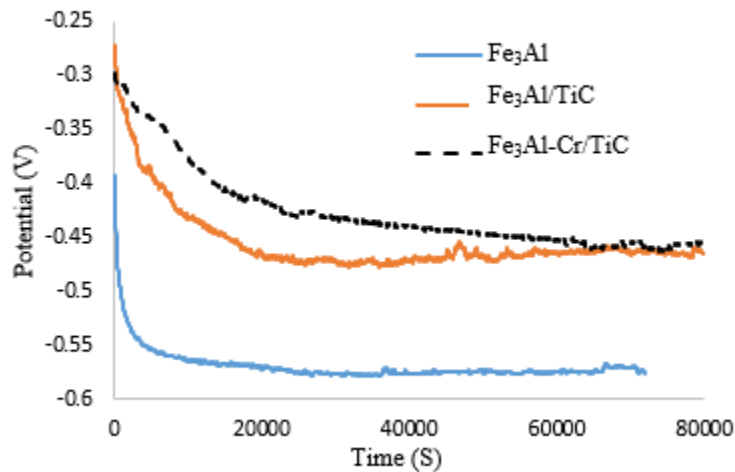


Fig. 22. Open circuit potential of Fe_3Al , $\text{Fe}_3\text{Al}/\text{TiC}$ and $\text{Fe}_3\text{Al-Cr}/\text{TiC}$ measured for 24 hours in freely aerated 3.5 wt.% NaCl

4.2. Potentiodynamic polarization

Fig. 23 presents the polarization curves of three coatings in a freely aerated solution of 3.5 wt.% NaCl. All samples demonstrate the similar shape of polarization curve. For the composite coatings ($\text{Fe}_3\text{Al}/\text{TiC}$ and $\text{Fe}_3\text{Al-Cr}/\text{TiC}$) the corrosion potential E_{corr} is nobler and the corrosion current I_{corr} is less than that of the Fe_3Al . This observation is in accordance with the OCP results. Although the current density remains constant beyond a certain potential, the curves demonstrate an active-passive behaviour where the anodic current rapidly increased to reach a region with very little change in its value with the increase of potential (passive region). However, no breakdown potential can be observed even in relatively high potentials.

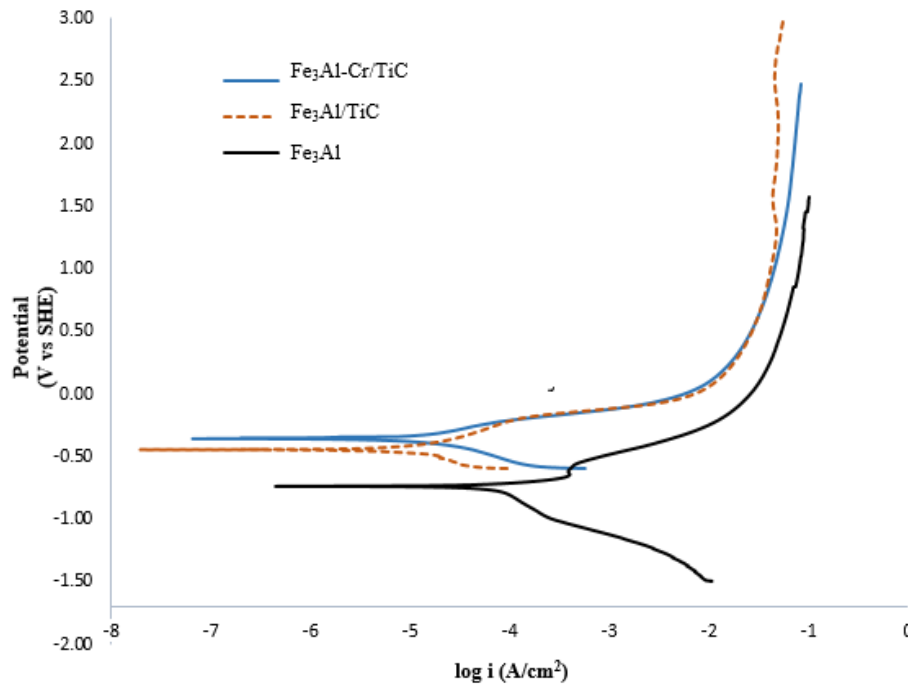


Fig. 23. The potentiodynamic polarization curves of Fe_3Al , $\text{Fe}_3\text{Al}/\text{TiC}$ and $\text{Fe}_3\text{Al-Cr}/\text{TiC}$ in freely aerated 3.5 wt% NaCl.

The values of corrosion parameters obtained from the polarization curves, such as cathodic Tafel (β_c) and anodic Tafel (β_a) slopes, the corrosion potential (E_{corr}), corrosion current density (j_{corr}) and polarization resistance is calculated using Stern-Geary method and are presented in Table 5. This It can be seen that by adding TiC particles to Fe_3Al matrix the anodic and cathodic current densities are decreased, and the value of the corrosion potential (E_{corr}) shifted to the less negative direction.

In composite coatings (Fe₃Al-TiC and Fe₃Al-Cr/TiC), a smaller value of J_{corr} and greater value of R_p , compared to those of Fe₃Al, suggest that the corrosion resistance of the composite coatings in 3.5 % NaCl solution has been improved by adding TiC and Cr. The corrosion rate of Fe₃Al-Cr/TiC composite is also almost 6 times less than that of the Fe₃Al sample.

Table 4. Polarization and corrosion parameters obtained from polarization curve of coatings in 3.5 % NaCl solution.

Sample	β_c (mV dec ⁻¹)	E_{corr} (mV)	β_a (V dec ⁻¹)	j_{corr} ($\mu\text{A cm}^{-2}$)	R_p ($\Omega \text{ cm}^2$)	R_{corr} (mm/Y)
Fe ₃ Al	350	-780	250	83.8	15.276	7.66×10^{-9}
Fe ₃ Al/TiC	380	-480	380	13.9	300	1.4×10^{-9}
Fe ₃ Al-Cr/TiC	170	-350	250	9.9	205	0.4×10^{-9}

4.3. Electrochemical impedance spectroscopy (EIS)

Electrochemical impedance spectroscopy (EIS) measurements were performed in order to study the mechanism of corrosion. The Nyquist diagrams after one hour of immersion are represented in the in **Fig. 25**. Compared to Fe₃Al, the composite coatings (Fe₃Al/TiC and Fe₃Al-Cr/TiC) exhibit higher impedance values, as indicated by the large diameter of the arc, indicating that the corrosion products layer formed on the surface is more protective than that formed on Fe₃Al [81]. This result is in good agreement with the results obtained by the potentiodynamic tests.

Fig. 25 highlights two types of diagrams. The first type is relative to Fe₃Al and Fe₃Al/TiC and consists of two overlapped capacitive loops. The time constant at high frequencies is attributed to the corrosion products layer while the second at intermediate and low frequencies is ascribed to the faradaic charge transfer process [82].

Among three coatings, Fe₃Al-Cr/TiC shows a different type of Nyquist diagram and exhibits a much larger impedance, as evidenced by a very large diameter of the arc. This increase of impedance is due to the addition of Cr to Fe₃Al/TiC since it is the only parameter being changed in this sample. The diagram consists of a semicircle, tended to be a straight line with a slope angle of around 45° (after $Z_{\text{real}} = 500$). An angle higher than 45° is reported as a characteristic of a diffusion process, corresponding to a concentration gradient localized in a porous layer and in the solution while semicircle curves are attributed to a charge transfer process [81]. Therefore, this

response for Fe₃Al-Cr/TiC could be the characteristic of a diffusion process while the semicircle curves of Fe₃Al and Fe₃Al/TiC are attributed to a charge transfer process.

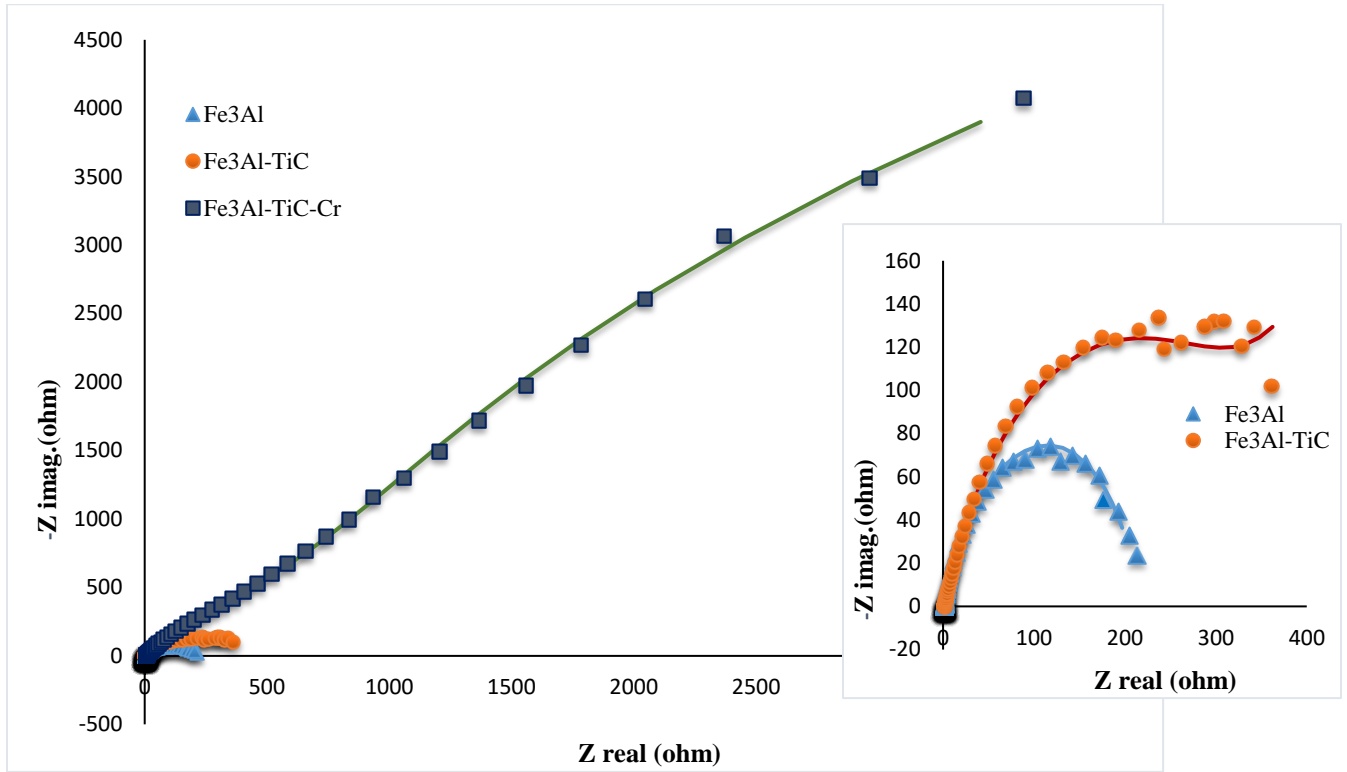


Fig. 24. Nyquist plot of Fe₃Al, Fe₃Al/TiC and Fe₃Al-Cr/TiC composite coatings after one-hour immersion in 3.5 % NaCl solution

In order to provide quantitative support to the experimental EIS results, an equivalent circuit was adopted, as shown in **Fig. 25**. The related impedance parameters were obtained by ZView software. The simulated curves (solid curves) are superposed to the experimental data in **Fig. 24**. As it can be seen, a very good agreement can be observed between the experimental and the simulated plots.

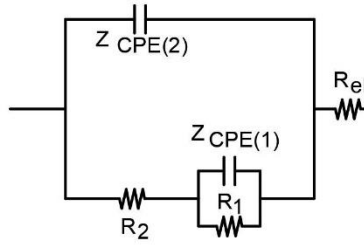


Fig. 25. The proposed equivalent circuit model used to obtain impedance.

The significance of the elements of the proposed equivalent circuit has been reported in the literature [29, 82]. In this circuit, R_{el} corresponds to the resistance of the electrolyte while R_2 and CPE_2 represent the resistance and the capacitance of the corrosion product layer, respectively. R_1 represents the charge transfer resistance, and CPE_1 represents double-layer capacitance. A constant phase element (CPE) was used to consider a deviation from an ideal capacitor. The origins of the CPE were summarised by Jorcin et al. [83], which includes distributed surface roughness and heterogeneity, slow adsorption reaction, non-uniform potential and current distribution. The relevant impedance of CPE is defined as:

$$CPE = Y_0 (j\omega)^n \quad (17)$$

Where Y_0 is the capacitance, $j\omega$ is a complex variable for sinusoidal perturbations with $\omega = 2\pi f$, and n is the frequency power of CPE . The value of n suites between -1 and 1. CPE can represent pure resistance for $n=0$, pure capacitance for $n=1$, Warburg impedance for $n=0.5$ and inductance for $n=-1$ [29].

Table 5. Impedance fit parameters for Fe₃Al, Fe₃Al-TiC and Fe₃Al-Cr/TiC.

Sample	R_{el} ($\Omega \text{ cm}^2$)	R_2 ($\Omega \text{ cm}^2$)	$(CPE_2) Y_{02}$ ($S \text{ cm}^{-2} s^n$)	n_2	R_1 ($\Omega \text{ cm}^2$)	$(CPE_1) Y_{01}$ ($S \text{ cm}^{-2} s^n$)	n_1
Fe ₃ Al	1.8688	187.3	7.962×10^{-3}	0.788	27.65	70×10^{-3}	1
Fe ₃ Al-TiC	1.807	356.9	3.413×10^{-3}	0.722	1.606×10^6	4.518×10^{-4}	0.579
Fe ₃ Al-Cr/TiC	7.188	1979	8.729×10^{-6}	0.883	16.77×10^3	0.785×10^{-3}	0.812

Considering the suggested equivalent circuit model, all measured impedance values for Fe₃Al, Fe₃Al-TiC and Fe₃Al-Cr/TiC are listed in **Table 5**. The calculated parameters indicate that the values of the fractional exponent, n_2 , for all specimens, are close to 1, being near to that of a pure capacitance. CPE_2 possesses physical meaning of the capacitance of the corrosion products layer. According to the Equation 18, the capacitance is proportional to the area of overlap (A) and is inversely proportional to the separation between the conducting sheets (d), where ϵ_r is the relative static permittivity and ϵ_0 is the vacuum permittivity. CPE_2 is thus considered to be inversely proportional to the thickness of the corrosion product (d).

$$C = \epsilon_r \epsilon_0 \frac{A}{d} \quad (18)$$

The CPE_2 values for composite coatings (Fe₃Al-TiC and Fe₃Al-Cr/TiC) are less than that of Fe₃Al. This result could be due to an increase of the thickness of the corrosion product layer or its composition change. R_2 value is also higher for the composite samples, compared to the pure Fe₃Al. This value significantly increases by adding Cr into the composite. The increase of the resistance of the corrosion products layer, R_2 , for composite coatings indicates that the corrosion products layers are more resistant to electron transfer. This could be an indication of the compactness of this layer. More compact corrosion products layer can block the dissolution reaction, providing an effective barrier against corrosion, therefore, among the composite samples, the corrosion product resistance of Fe₃Al-Cr/TiC is much greater than that of Fe₃Al-TiC.

The charge transfer resistance, R_1 of $\text{Fe}_3\text{Al}/\text{TiC}$ is also higher than that of the two other samples which is likely due to the blocking effect of the more compact corrosion products layer formed at the surface. R_1 for composite coatings ($\text{Fe}_3\text{Al}/\text{TiC}$ and $\text{Fe}_3\text{Al-Cr}/\text{TiC}$) are considerably higher than that of Fe_3Al .

As a summary, EIS measurements confirmed that a fairly protective surface layer is formed on all samples after one-hour exposure to naturally aerated 3.5 % NaCl solution. However, the more compact surface layer was formed on $\text{Fe}_3\text{Al-Cr}/\text{TiC}$, and the corrosion mechanism is diffusion process. $\text{Fe}_3\text{Al}/\text{TiC}$ and Fe_3Al exhibited charge transfer mechanism.

4.4. Possible corrosion reactions

Before analysing the surface, the possible reactions of iron aluminide as the matrix of composite and TiC as reinforcement are reviewed. According to previous works on iron aluminide [1],

during active dissolution the following reactions may take place:



After active dissolution from iron aluminide, aluminium quickly converts into Al_2O_3 on the surface by following reaction, whereas iron ions remain in the solution.



Contrary to the oxide film on a pure aluminum, this Al_2O_3 layer is not continuous and exhibits a porous structure. The porosity allows the corrosion process to continue and iron dissolves from the surface. Therefore, FeO and Fe_2O_3 iron oxides start to form on the surface.



More Al-OH formed by the following reaction:



The role of TiC in passivation in 3 % NaCl solution was explained by Lavrenko et al. [84]. TiC, owed to the high value of the oxygen adsorption energy on its surface has good corrosion resistance. They revealed that electrolytic corrosion of TiC, in 3 % NaCl solution, is a multistep process. After an initial anodic dissolution, with the transfer of Ti^{3+} and TiO^{2+} ions into the solution, the formation of TiO_2 (rutile) partially protecting layers, slows down the dissolution of the composites.



Corrosion products consist of the intermediate scale layer composed of the TiO lower oxide while the external layer is composed of rutile TiO_2 .

4.5. SEM and EDS Analyses

Post corrosion analyses were performed to study the surface of the samples after corrosion. The analyses consist of microstructural analysis with scanning electron microscopy (SEM), equipped by EDS elemental. The Passive layer of the samples, after being polarized from -1 to +1.5 V (vs. OCP), were examined. SEM images have shown that the effective corrosion mechanism is a uniform attack. **Fig. 26** shows the surface morphology of the samples after potentiodynamic polarization test exposure to 3.5 % NaCl solution. A thick layer of corrosion products (including passive layer) covers the entire surface of the coatings. The corrosion products were different for the studied samples, both in colour and in composition. For the elemental analysis of passive layer, Energy Dispersive Spectroscopy (EDS) related to each SEM images was performed.

EDS results show an approximate amount of each element in the passive layer. In Fe_3Al sample, Fe, Al and O are detected in the passive layer, but hydrogen amount cannot be detected by this method. The weight percent calculation indicates a large amount of O and C in the passive layer. However, this elemental analysis does not give any information about the type of compounds and the mechanisms of passivation. In order to achieve these goals, XPS analysis was performed.

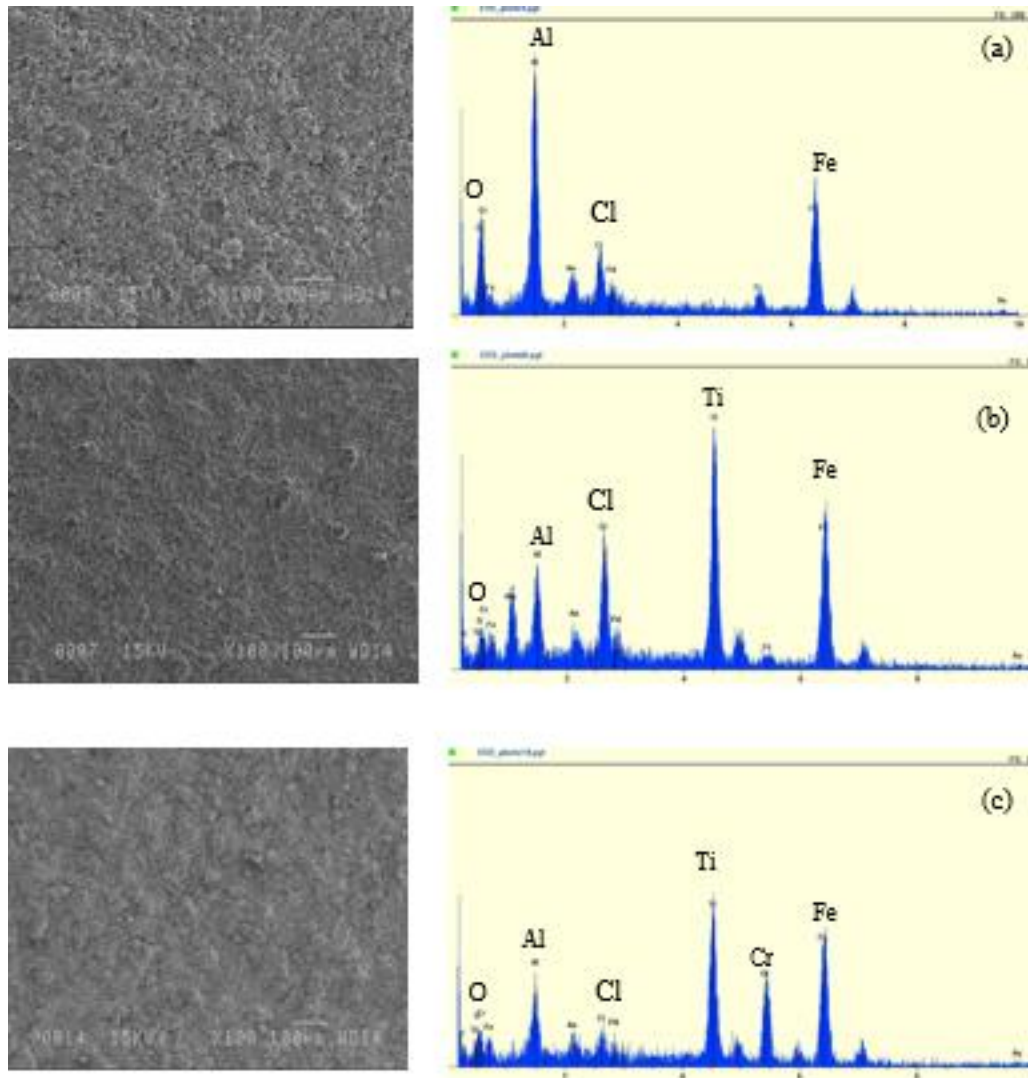


Fig. 26. SEM micrograph and related EDS analysis of the passive layer formed on (a) Fe_3Al , $\text{Fe}_3\text{Al}/\text{TiC}$ (b) and $\text{Fe}_3\text{Al-Cr}/\text{TiC}$ (c) after potentiodynamic test exposure to 3.5 % NaCl solution.

4.6. XPS Analysis

Samples of three coatings before polarization test and after passivation in 3.5 % NaCl solution were analyzed by XPS technique to investigate the passive layer compounds. This analysis was included Fe, Al, Ti, Cl, O, Cr and Na as major elements in the passive layer.

XPS spectra of the passive layer after polarization of the coatings are illustrated in **Fig.s 27-31**. In **Fig. 27**, XPS spectra of Fe, for Fe_3Al (a), $\text{Fe}_3\text{Al}/\text{TiC}$ (b) and $\text{Fe}_3\text{Al-Cr}/\text{TiC}$ (c) was presented.

Appearing of the peak in the passive layer of coatings at 710.7 eV is associated with Fe^{+3} . Satellite at 743.2 eV is characteristic of the Fe^{+3} state, and positions of satellites 2 and 3 in agreement with the Fe^{+3} state. In **Fig. 27-b**, visually detectable Fe^{+2} satellites can be seen, and it is an evidence of the mixture of Fe^{+3} and Fe^{+2} .

In **Fig. 28**, XPS spectra of Al, before the test (a) and after passivation (b) are illustrated. The appearance of the peak at 74.7 eV in the sample before corrosion (a) is assigned to the binding energy of Al^{3+} in Al_2O_3 . This oxide could be formed during HVOF technique by the exposure of pure aluminum to air. In the case of the passivated sample (b), there is a shift in the Al^{3+} peak towards high binding energy. By deconvolution of the spectra, it was revealed the coexistence of Al^{3+} as Al_2O_3 , $\text{Al}(\text{OH})_3$ and AlCl_3 at 74.7, 75 and 77.29 eV, respectively [75].

This results for Al and Fe is similar to what Frangini et al. [58] reported while comparing oxidized and passivated iron aluminide samples. They reported that the outer part of the passive film predominantly consists of mixed Al-Fe oxy-hydroxide whereas the inner part is of mostly an Al-rich oxide phase.

Fig. 29 presents the XPS spectra of Ti2p in a passive layer of two composites, $\text{Fe}_3\text{Al}/\text{TiC}$ (a) and $\text{Fe}_3\text{Al-Cr}/\text{TiC}$ (b). Two spectra are almost the same and are attributed to $\text{Ti}2p_{1/2}$ and $\text{Ti}2p_{3/2}$ and are compatible to TiO and TiO_2 . However binding energy that is attributed to TiC is 454.9-455.1 eV, and that could be confused with TiO . XPS spectra of Cr2p, in **Fig. 31**, is attributed to $\text{Cr}(\text{OH})_3$ that is formed in the passive layer.

These results indicate that the passive layer of composite coatings ($\text{Fe}_3\text{Al}/\text{TiC}$ and $\text{Fe}_3\text{Al-Cr}/\text{TiC}$) consists of a mixture of aluminum, iron and titanium oxide and aluminum hydroxide. In case of $\text{Fe}_3\text{Al-Cr} / \text{TiC}$, chromium hydroxide also exists in the passive layer. The presence of hydroxide could be the result of hydration of passive film that can happen by raising potential [23].

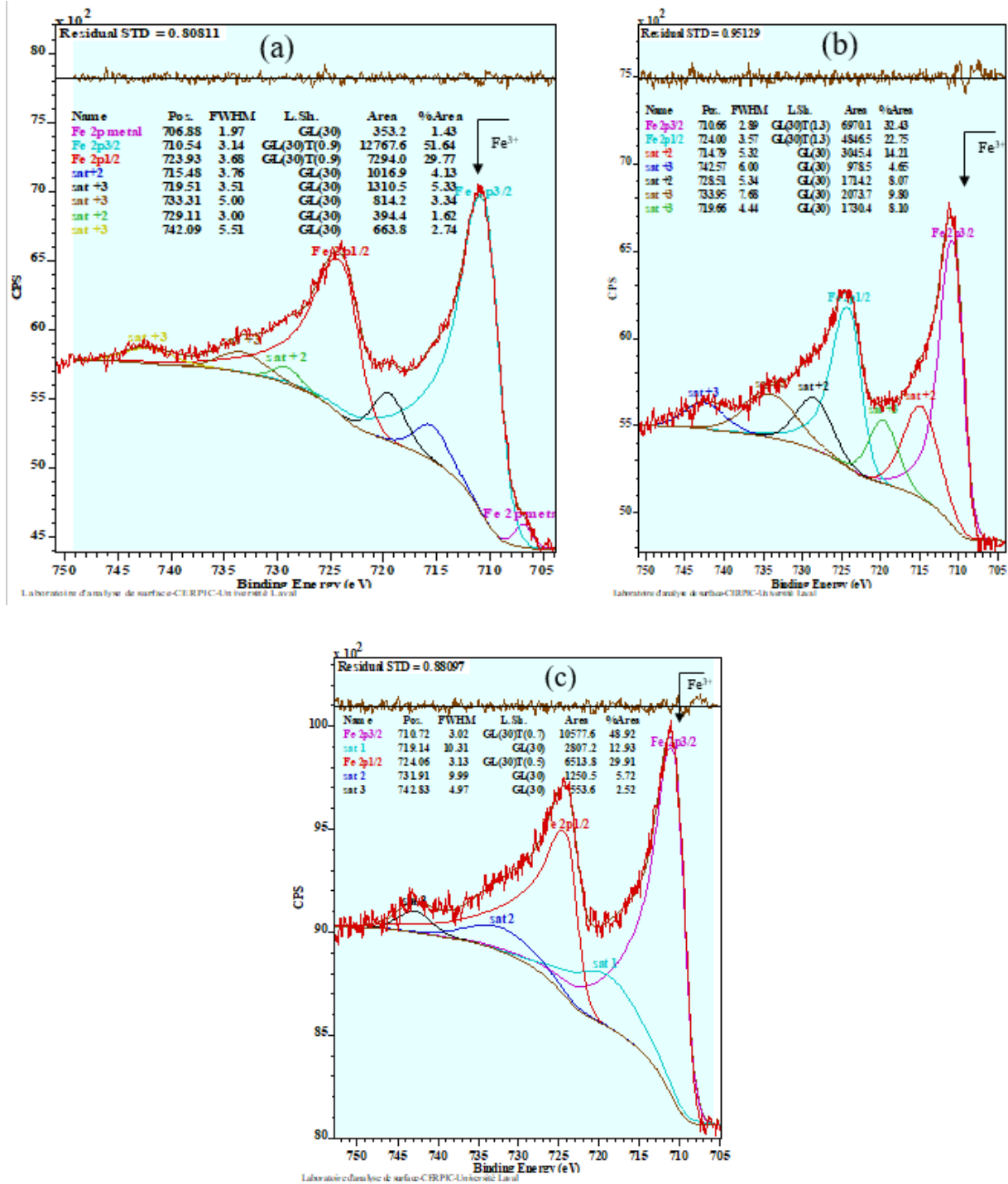


Fig. 27. XPS Spectra for Fe 2p for (a)Fe₃Al (b) Fe₃Al/TiC and (c)Fe₃Al-Cr/TiC.

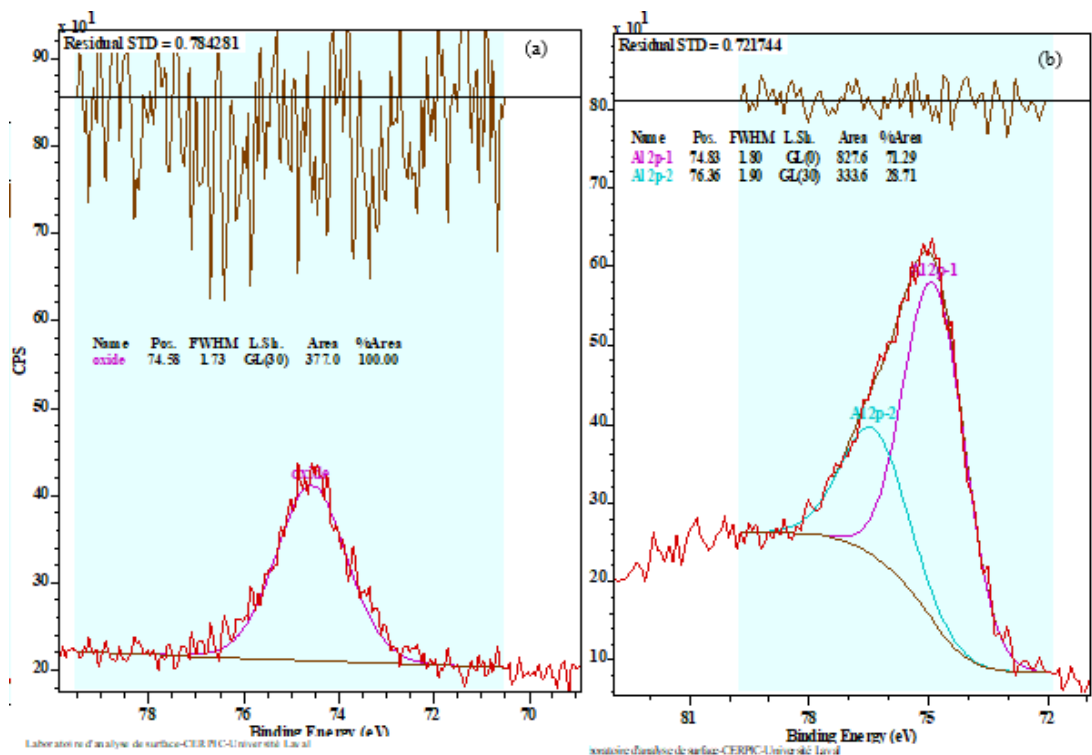


Fig. 28. XPS spectra of Al 2p (a) before polarization test and (b) passivated sample.

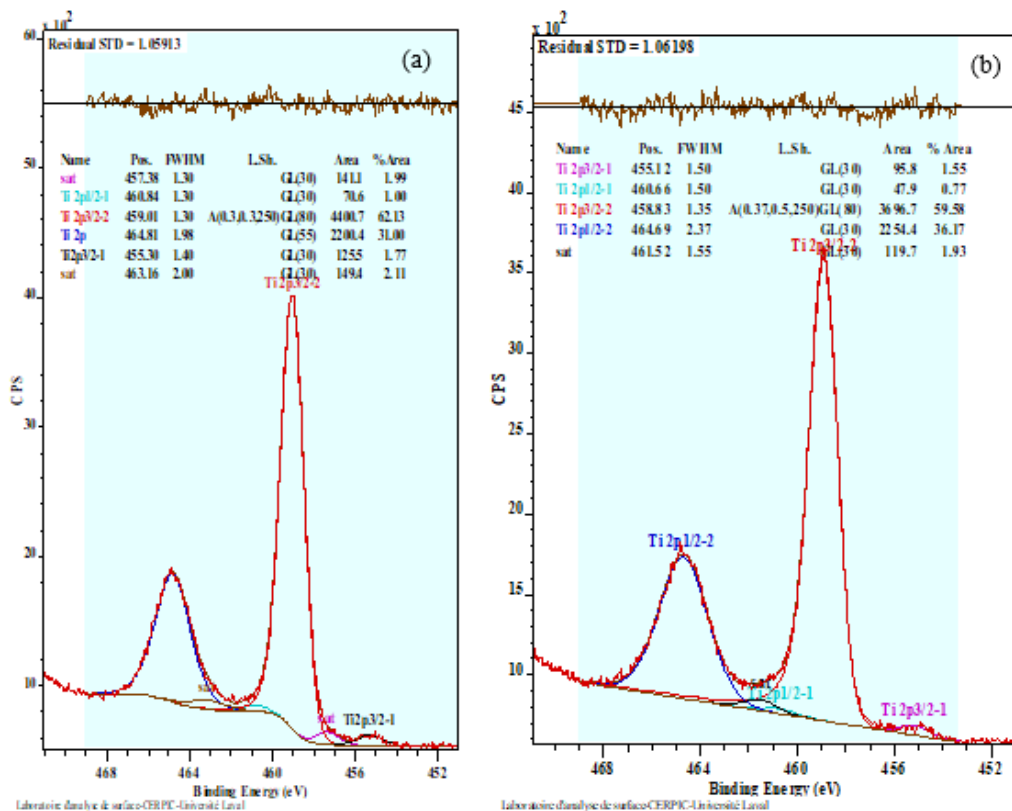


Fig. 29. XPS spectra of Ti2p (a) Fe₃Al/TiC (b) Fe₃Al-Cr/TiC.

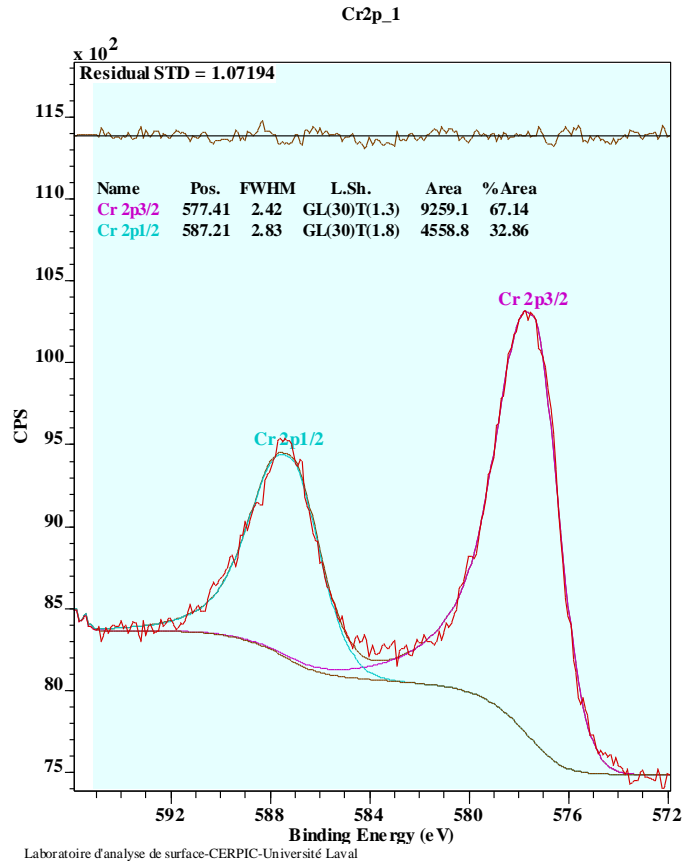


Fig. 30. XPS spectra of Cr 2p Fe₃Al-Cr/TiC.

Elemental analyses, extracted from XPS spectra of three coatings, before and after passivation tests during potentiodynamic polarization test in 3.5 % NaCl solution, are presented in Table 7 and Fig. 32. A large amount of oxygen in coatings before the test could be due to the oxidation during applying the coating by HVOF technique or natural oxidation in contact with air. Fe₃Al surface analysis revealed iron and aluminum oxides and chlorides (Table 7) on the surface. The concentration of Al on the surface increased substantially after corrosion, while that of iron slightly decreased. This is in good agreement with the results reported by Shankar Rao [23] stating that Al gets enriched on the surface with the dissolution of the alloy, in the form of oxide and chloride, whereas Fe goes into the solution. This is because Al₂O₃ has thermodynamically more stable compared to iron oxide and kinetically and the mobility of Al³⁺ ion is low compared to Fe³⁺ ion within the barrier film [23].

Table 6. Elemental analysis results of the surface before the test after passivation in 3.5% NaCl solution during the potentiodynamic test.

at. %	Fe ₃ Al		Fe ₃ Al/TiC		Fe ₃ Al-Cr/TiC	
	Before the test	passivated	Before the test	passivated	Before the test	passivated
Fe	6.13	4.44	5.71	6.37	2.94	6.27
Al	3.91	13.07	3.6	2.88	2.52	1.46
Ti	0	0	1.1	7.43	0	6.96
Cr	0.3	0.86	0.21	1.82	1.9	4.33
O	40	53.72	46.14	47.37	31.12	44.41
Cl	1.64	22.34	1.01	30.11	3.59	2.4

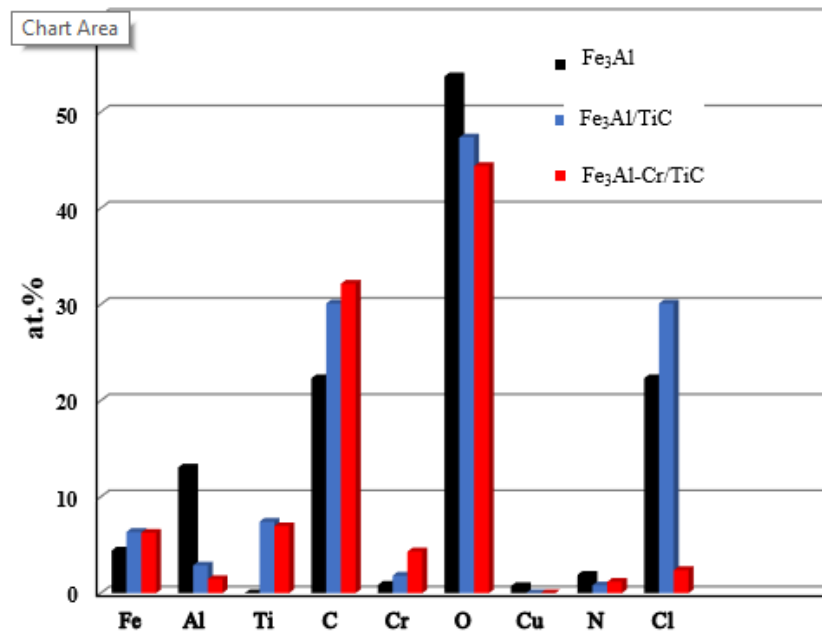


Fig. 31. Elemental analysis results of the surface after passivation in 3.5 % NaCl solution during the potentiodynamic test.

In case of Fe₃Al/TiC, high amount of Ti after corrosion could indicate that TiC dissolved in solution according to equations (26) and (27). Thus, Ti remained in the passive layer in the form of TiC, TiO, and TiO₂ (oxidation usually takes place during HVOF process) and its concentration increases, as the corrosion progresses. Comparing two composites, in case of Fe₃Al-Cr/TiC, the passive layer consists of less chloride that is good evidence of better protection. As discussed by

Zamanzadeh [48], Cr^{3+} may substitute the Al^{3+} site. During the formation of the passive film, Cr^{3+} diffuses into the solution/oxide interface. They may segregate at the crystal imperfection sites which act as the entry sites for the chloride ions because of the high surface energy of the defects. Thus, the entry site may be blocked by the Cr oxide and therefore reduce the penetration of chloride ions.

4.7. Cyclic Polarization

Cyclic polarization is a variant of the potentiodynamic polarization technique, and it is widely used to determine the tendency of specific materials towards pitting corrosion. In this work, cyclic polarization tests were performed in sulphuric acid solution to study the passivation and pitting behaviour of the coatings .

Fig. 33 presents cyclic potentiodynamic polarization curves of coatings in 0.25 M sulphuric acid solution. The shape of diagrams for Fe_3Al and $\text{Fe}_3\text{Al}/\text{TiC}$ is in good agreement with other works about iron aluminides [28, 29, 31, 86] which consists of several partial passivation and breakdown.

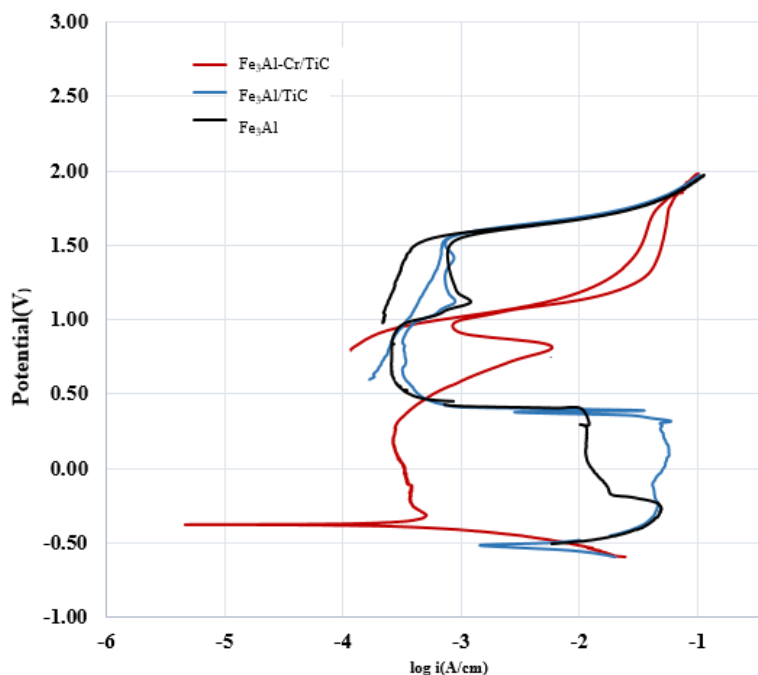


Fig. 32. Cyclic polarization diagram of Fe_3Al , $\text{Fe}_3\text{Al}/\text{TiC}$ and $\text{Fe}_3\text{Al-Cr}/\text{TiC}$ coating in 0.25 M sulphuric acid solution

As shown in Fig. 33, the individual coatings exhibited cyclic polarization curves, with clockwise hysteresis loops which are extremely small in case of Fe_3Al and $\text{Fe}_3\text{Al}/\text{TiC}$. The potential at which the

current sharply increases is defined as the passivation breakdown potential (E_b) or pitting potential (E_{pit}) and the potential at which the loop closes on the reverse scan is the protection or re-protection potential (E_p). In case of Fe_3Al and Fe_3Al/TiC samples, these two potentials are the same, and there is no tendency to pitting. Fe_3Al-Cr/TiC shows more positive E_p than E_b , therefore, there is a little tendency to pitting. Furthermore, the size of the pitting loop can be used as an indication of pitting tendency. The larger loop in Fe_3Al-Cr/TiC shows more tendency to pitting.

Corrosion and cyclic polarization parameters of Fe_3Al , Fe_3Al/TiC and Fe_3Al-Cr/TiC in 0.25 M sulphuric acid solution are presented in Table 8. Composite coatings, with less negative corrosion potential (E_{corr}) and less corrosion current, revealed better corrosion parameters than did Fe_3Al . In fact, the corrosion current of Fe_3Al/TiC is slightly lower than that of Fe_3Al while the addition of Cr (Fe_3Al-Cr/TiC sample) exhibits a much lower corrosion current which is 27 times smaller than that of Fe_3Al . However, in the case of Fe_3Al-Cr/TiC , compared to the other coatings, the difference between corrosion potential and breakdown potential (E_b-E_{corr}) has smaller value, and the passive breakdown occurs in more negative potential. This displays less pitting resistance of this coating in sulphuric acid solution. Furthermore, once a pit formed, it propagates at a faster rate in Fe_3Al-Cr/TiC , as indicated by the higher active current.

Table 7. Cyclic polarization parameters of Fe_3Al , Fe_3Al/TiC and Fe_3Al-Cr/TiC in 0.25 M sulphuric acid solution

	E_{corr} (mV)	i_{corr} (mA/cm ²)	E_b (mV)	E_p (mV)	$E_b - E_{corr}$ (mV)
Fe_3Al	-518	11.64	1490	1590	2008
Fe_3Al/TiC	-500	9.27	1487	1.58	1987
Fe_3Al-Cr/TiC	-380	0.42	1010	1.103	1390

Results of potentiodynamic cyclic polarization revealed that adding TiC to Fe_3Al does not have a negative effect on the corrosion resistance of Fe_3Al . On the other hand, it was reported that [28, 86] adding chromium in small amounts (2-5 at.%) may improve the pitting resistance of Fe_3Al in a mixed solution of Na_2SO_4 and $NaCl$. Our results did not show such a clear tendency. Fe_3Al-Cr/TiC composite coating did not exhibit good resistance to pitting in sulphuric acid solution, although its general corrosion resistance is significantly improved by Cr addition.

CONCLUSION AND OUTLOOK

5.1. General Conclusion

The corrosion behaviour of two composite coatings with the Fe₃Al matrix, prepared by high-velocity oxy-fuel (HVOF) spraying, in 3.5 wt.% NaCl was studied. The effect of chromium addition on corrosion behaviour of the coatings was evaluated. Electrochemical measurements such as electrochemical impedance spectroscopy and potentiodynamic polarization were considered to examine corrosion behaviour of Fe₃Al, Fe₃Al/TiC and Fe₃Al-Cr/TiC coatings. Furthermore, cyclic polarization test in 0.25 M sulphuric acid was performed to study the pitting resistance of the coatings. Post-corrosion analysis such as scanning electron microscopy (SEM) and X-ray photoelectron spectroscopy (XPS) was employed to characterize the passive layer that formed during polarization in order to provide useful and complementary data and explanations. According to the research work during this project, the following conclusions can be drawn:

- 1- An oxide layer is formed on the surface of all coatings before corrosion tests. This layer could be formed due to oxidation of the sample during HVOF process or by natural oxidation in the air. In OCP tests, a decrease of potential toward negative potential with time is evidence of dissolution of this pre-corrosion film. After a while, the potential shows a good stabilization, due to the formation of the stable passive layer.
- 2- Potentiodynamic polarization revealed that two composite coatings (Fe₃Al/TiC and Fe₃Al-Cr/TiC), with smaller corrosion current density (i_{corr}) and more positive corrosion potential (E_{corr}), exhibit better corrosion performance than does Fe₃Al. The corrosion rate of Fe₃Al/TiC is almost 6 times higher than that of Fe₃Al in 3.5 % NaCl solution.
- 3- The Nyquist plot of EIS revealed that Fe₃Al-Cr/TiC shows a different type of diagram with much larger impedance, comparing to the other coatings. This increase of impedance could be due to the addition of Cr to Fe₃Al/TiC. The diagram consists of a semicircle tended to be a straight line with a slope angle of around 45°. An angle higher than 45° was reported as a characteristic of a diffusion process, corresponding to a concentration gradient localized in a porous layer. This response for Fe₃Al-Cr/TiC could, therefore, be the characteristic of a diffusion process while the semicircle curves of Fe₃Al and Fe₃Al/TiC are attributed to a charge transfer process.

- 4- SEM images of the surface of coatings after polarization test show general uniform corrosion and no localized corrosion was detected.
- 5- XPS spectra of passive layer after polarization revealed the existence of iron, aluminum oxides and hydroxide plus titanium oxide that could be mixed with titanium carbide. Elemental analysis shows that the passive layer of Fe₃Al-Cr/TiC consists of less chloride comparing to that of Fe₃Al/TiC and it is good evidence of better protection. During the formation of the passive film, Cr³⁺ diffuses into the solution/oxide interface. They may segregate at the crystal imperfection sites which act as the entry sites for the chloride ions because of the high surface energy of the defects. Thus, the entry sites are blocked by the Cr oxide and therefore reduce the penetration of chloride ions.
- 6- Cyclic polarization tests performed in 0.25 M sulphuric acid solution due to study the passivation and pitting behaviour of coatings in a different solution to compare the results of several other works on iron aluminides in this solution. Results of potentiodynamic cyclic polarization revealed that adding TiC to Fe₃Al does not have a significant effect on corrosion behaviour of Fe₃Al. However, in case of Fe₃Al-Cr/TiC, the difference between corrosion potential and breakdown potential, ($E_b - E_{corr}$) has a smaller value, and the passive breakdown occurs in more negative potential which displays less pitting resistance of this coating in sulphuric acid solution. Furthermore, once a pit formed, it propagated at a fast rate in Fe₃Al-Cr/TiC as indicated by the higher active current.

These results revealed that adding TiC particles to Fe₃Al matrix to improve the wear resistance does not deteriorate the corrosion behaviour of Fe₃Al coating. The addition of Cr in Fe₃Al/TiC composite coatings could further improve their corrosion resistance. However, in sulphuric acid solution, this coating exhibits low pitting resistance.

5.2. Outlook

Based on the obtained results in this research study, the following perspectives and future work could be considered

1. Electrochemical studies including OCP, potentiodynamic polarization and electrochemical impedance in a mixed solution of H₂SO₄ and NaCl or other solutions to study the role of chloride ion in corrosion behaviour of the composite.
2. Post corrosion investigation such as chemical analysis of passive layer by XPS technique to evaluate passive layer that formed on the coatings in a different solution.
3. Performing Electrochemical studies in dynamic solution to approach to the real condition that an industrial part such as turbine blade works.

6. References

1. Rao, V.S., *A review of the electrochemical corrosion behaviour of iron aluminides*. *Electrochimica Acta*, 2004. **49**(26): p. 4533-4542.
2. Zamanzade, M., A. Barnoush, and C. Motz, *A Review on the Properties of Iron Aluminide Intermetallics*. *Crystals*, 2016. **6**(1): p. 10.
3. Cinca, N., C.R.C. Lima, and J.M. Guilemany, *An overview of intermetallics research and application: Status of thermal spray coatings*. *Journal of Materials Research and Technology*, 2013. **2**(1): p. 75-86.
4. Amiriyan, M., et al., *Dry sliding wear behavior of Fe₃Al and Fe₃Al/TiC coatings prepared by HVOF*. *Wear*, 2015. **342-343**: p. 154-162.
5. Xu, B., et al., *Sliding wear behavior of Fe–Al and Fe–Al/WC coatings prepared by high velocity arc spraying*. *Wear*, 2004. **257**(11): p. 1089-1095.
6. ZHU, Z.-x., et al., *Influence of Heat Treatment on Microstructure and Wear Behavior of Fe-Al/WC Composite Coatings [J]*. *Journal of Materials Engineering*, 2004. **7**: p. 000.
7. Durlu, N., *Titanium carbide based composites for high temperature applications*. *Journal of the European Ceramic Society*, 1999. **19**(13): p. 2415-2419.
8. Hussainova, I., *Some aspects of solid particle erosion of cermets*. *Tribology international*, 2001. **34**(2): p. 89-93.
9. Chen, Y. and H. Wang, *Microstructure and wear resistance of laser clad TiC reinforced FeAl intermetallic matrix composite coatings*. *Surface and Coatings Technology*, 2003. **168**(1): p. 30-36.
10. Kumar, S., et al., *Characterization and comparison between ball milled and plasma processed iron-aluminium thermal spray coatings*. *Surface and Coatings Technology*, 2006. **201**(3–4): p. 1267-1275.
11. Song, B., et al., *Oxidation Control of Atmospheric Plasma Sprayed FeAl Intermetallic Coatings Using Dry-Ice Blasting*. *Journal of Thermal Spray Technology*, 2013. **22**(2): p. 345-351.
12. *High-Temperature Sulfidation of Fe₃Al Thermal Spray Coatings at 600°C*. *CORROSION*, 2000. **56**(2): p. 189-198.
13. Frangini, S. and A. Masci, *Intermetallic FeAl based coatings deposited by the electrospark technique: corrosion behavior in molten (Li+K) carbonate*. *Surface and Coatings Technology*, 2004. **184**(1): p. 31-39.
14. Pokhmurska, H., et al., *Tribological properties of arc sprayed coatings obtained from FeCrB and FeCr-based powder wires*. *Surface and Coatings Technology*, 2002. **151–152**: p. 490-494.
15. Szczycka-Lasota, B., et al., *Oxidation models of the growth of corrosion products on the intermetallic coatings strengthened by a fine dispersive Al₂O₃*. *Journal of Materials Processing Technology*, 2005. **164–165**: p. 935-939.
16. Sidhu, T., S. Prakash, and R. Agrawal, *Studies on the properties of high-velocity oxy-fuel thermal spray coatings for higher temperature applications*. *Materials Science*, 2005. **41**(6): p. 805-823.
17. Rosalbino, F., et al., *Effect of silicon and germanium alloying additions on the passivation characteristics of Fe₃Al intermetallic in sulphuric acid solution*. *Electrochimica Acta*, 2012. **62**: p. 305-312.
18. Chiang, W.-C., W.-C. Luu, and J.-K. Wu, *Effect of aluminum content on the passivation behavior of Fe–Al alloys in sulfuric acid solution*. *Journal of materials science*, 2006. **41**(10): p. 3041-3044.
19. Sharma, G., et al., *Aqueous corrosion behavior of iron aluminide intermetallics*. *Journal of Materials Engineering and Performance*, 2007. **16**(6): p. 779-783.

20. Porcayo-Calderon, J., et al., *Corrosion performance of Fe-Al intermetallic coatings in 1.0 M NaOH solution*. Int. J. Electrochem. Sci, 2013. **8**(11): p. 12205-12218.
21. Ji, G., O. Elkedim, and T. Grosdidier, *Deposition and corrosion resistance of HVOF sprayed nanocrystalline iron aluminide coatings*. Surface and Coatings Technology, 2005. **190**(2): p. 406-416.
22. Liu, T., et al., *The electrochemistry corrosion behavior of Fe₃Al-type intermetallic with super-hydrophobic surfaces*. Materials and Manufacturing Processes, 2010. **25**(5): p. 298-301.
23. Rao, V.S., *Repassivation behaviour and surface analysis of Fe₃Al based iron aluminide in 0.25 M H₂SO₄*. Corrosion science, 2005. **47**(1): p. 183-194.
24. Huape-Padilla, E., et al., *Corrosion study of Fe-Al Intermetallic Alloys in Simulated Acid Rain*. Int. J. Electrochem. Sci, 2015. **10**: p. 2141-2154.
25. Amiriyani, M., et al., *Dry sliding wear behavior of Fe₃Al and Fe₃Al/TiC coatings prepared by HVOF*. Wear, 2015. **342**: p. 154-162.
26. Amiriyani, M., et al., *Mechanical Behavior and Sliding Wear Studies on Iron Aluminide Coatings Reinforced with Titanium Carbide*. Metals, 2017. **7**(5): p. 177.
27. Rosalbino, F., et al., *Investigation of passivity and its breakdown on Fe₃Al–Si and Fe₃Al–Ge intermetallics in chloride-containing solution*. Corrosion Science, 2014. **85**: p. 394-400.
28. Negache, M., et al., *Effect of Cr, Nb and Zr additions on the aqueous corrosion behavior of iron-aluminide*. Intermetallics, 2013. **36**: p. 73-80.
29. Rosalbino, F., et al., *Effect of copper alloying addition on the electrochemical corrosion behaviour of Fe₃Al intermetallic in sulphuric acid solution*. Materials and Corrosion, 2016. **67**(10): p. 1042-1048.
30. Zamanzade, M., H. Vehoff, and A. Barnoush, *Cr effect on hydrogen embrittlement of Fe₃Al-based iron aluminide intermetallics: Surface or bulk effect*. Acta materialia, 2014. **69**: p. 210-223.
31. Rao, V.S., R. Baligheid, and V. Raja, *Effect of carbon on corrosion behaviour of Fe₃Al intermetallics in 0.5 N sulphuric acid*. Corrosion Science, 2002. **44**(3): p. 521-533.
32. McKamey, C., J. Horton, and C. Liu, *Effect of chromium on properties of Fe₃Al*. Journal of Materials Research, 1989. **4**(05): p. 1156-1163.
33. Keddami, M., O.R. Mattos, and H. Takenouti, *Mechanism of anodic dissolution of iron-chromium alloys investigated by electrode impedances—I. Experimental results and reaction model*. Electrochimica Acta, 1986. **31**(9): p. 1147-1158.
34. Keddami, M., O. Mattos, and H. Takenouti, *Mechanism of anodic dissolution of iron-chromium alloys investigated by electrode impedances—II. Elaboration of the reaction model*. Electrochimica Acta, 1986. **31**(9): p. 1159-1165.
35. Epelboin, I., et al., *The dissolution and passivation of Fe and FeCr alloys in acidified sulphate medium: Influences of pH and Cr content*. Corrosion Science, 1979. **19**(7): p. 1105-1112.
36. Zamanzade, M. and A. Barnoush, *An overview of the hydrogen embrittlement of iron aluminides*. Procedia Materials Science, 2014. **3**: p. 2016-2023.
37. Novák, P., et al., *On the formation of intermetallics in Fe–Al system – An in situ XRD study*. Intermetallics, 2013. **32**(Supplement C): p. 127-136.
38. Taylor, A. and R. Jones, *Constitution and magnetic properties of iron-rich iron-aluminum alloys*. Journal of Physics and Chemistry of Solids, 1958. **6**(1): p. 16-37.
39. Bradley, A. and A. Jay, *The formation of superlattices in alloys of iron and aluminium*. Proceedings of the Royal Society of London. Series A, Containing Papers of a Mathematical and Physical Character, 1932. **136**(829): p. 210-232.
40. Lawley, A. and R. Cahn, *A high temperature X-ray study of ordering in iron-aluminium alloys*. Journal of Physics and Chemistry of Solids, 1961. **20**(3-4): p. 204-221.

41. Fu, C., *Origin of ordering in B2-type transition-metal aluminides: Comparative study of the defect properties of PdAl, NiAl, and FeAl*. Physical Review B, 1995. **52**(5): p. 3151.
42. Hasemann, G., et al., *Vacancy strengthening in Fe 3 Al iron aluminides*. Intermetallics, 2014. **54**: p. 95-103.
43. Yasuda, H., et al., *Effect of Al concentration on pseudoelasticity in Fe 3 Al single crystals*. Acta materialia, 2005. **53**(20): p. 5343-5351.
44. Yoshimi, K., S. Hanada, and M. Yoo, *Yielding and plastic flow behavior of B2-type Fe-39.5 mol.% Al single crystals in compression*. Acta metallurgica et materialia, 1995. **43**(11): p. 4141-4151.
45. Palm, M., *Concepts derived from phase diagram studies for the strengthening of Fe–Al-based alloys*. Intermetallics, 2005. **13**(12): p. 1286-1295.
46. Fu, C. and J. Zou, *Site preference of ternary alloying additions in FeAl and NiAl by first-principles calculations*. Acta materialia, 1996. **44**(4): p. 1471-1478.
47. McKamey, C., J. Horton, and C. Liu, *Effect of chromium on properties of Fe 3 Al*. Journal of Materials Research, 1989. **4**(5): p. 1156-1163.
48. Zamanzade, M. and A. Barnoush, *Effect of chromium on the electrochemical properties of iron aluminide intermetallics*. Corrosion Science, 2014. **78**: p. 223-232.
49. Balasubramaniam, R., *On the role of chromium in minimizing room temperature hydrogen embrittlement in iron aluminides*. Scripta materialia, 1996. **34**(1): p. 127-133.
50. Palm, M., *The Al–Cr–Fe system–Phases and phase equilibria in the Al-rich corner*. Journal of Alloys and Compounds, 1997. **252**(1): p. 192-200.
51. Morris, D., M. Dadras, and M. Morris, *The influence of chromium additions on order and ductility in Fe3Al intermetallic*. Le Journal de Physique IV, 1993. **3**(C7): p. C7-429-C7-434.
52. Ghali, E., V.S. Sastri, and M. Elboudjaini, *Corrosion prevention and protection: practical solutions*. 2007: John Wiley & Sons.
53. Schweitzer, P.A., *Fundamentals of corrosion mechanisms, causes, and preventative methods*. 2010, CRC Press: Boca Raton, Fla.
54. Schweitzer, P.A., *Fundamentals of corrosion : mechanisms, causes, and preventative methods*. 2010, Boca Raton, FL: CRC Press. xxiii, 403 p.
55. Frankel, G.S., *Fundamentals of Corrosion Kinetics*, in *Active Protective Coatings: New-Generation Coatings for Metals*, A.E. Hughes, et al., Editors. 2016, Springer Netherlands: Dordrecht. p. 17-32.
56. Revie, R.W. and H.H. Uhlig, *Uhlig's corrosion handbook*. 2011, Wiley: Hoboken, New Jersey.
57. Standard, A., *G59-97*. PA: ASTM, 2003.
58. Frangini, S., et al., *A combined electrochemical and XPS study on the passivity of B2 iron aluminides in sulphuric acid solution*. Corrosion science, 1997. **39**(8): p. 1431-1442.
59. Schaeppers, D. and H.-H. Strehblow, *An XPS and ISS investigation of passive layers on binary Fe-Al alloys*. Corrosion science, 1997. **39**(12): p. 2193-2213.
60. Schaeppers, D. and H.H. Strehblow, *Surface analytical investigations of electrochemically formed passive layers on binary Fe/Al alloys*. Journal of the Electrochemical Society, 1995. **142**(7): p. 2210-2218.
61. Schaeppers, D., et al., *Electrochemical, ellipsometrical and surface analytical investigations of passive layers on binary Fe/Al alloys*. Surface and interface analysis, 1994. **21**(6-7): p. 342-348.
62. Frangini, S., J. Lasovich, and N. De Cristofaro, *Pitting susceptibility of chromium modified passive films of a B2-FeAl intermetallic alloy*. in *Materials Science Forum*. 1995. Trans Tech Publ.
63. Ghali, E., *Corrosion resistance of aluminum and magnesium alloys : understanding, performance, and testing*. 2010, Hoboken, N.J: Wiley. xxi, 719 p.
64. Cottis, R.A. and L.L. Shreir, *Shreir's corrosion*. 4th ed ed. 2010, Amsterdam: Elsevier. 4 v.

65. Arrieta-Gonzalez, C., et al., *Electrochemical behavior of Fe₃Al modified with Ni in Hank's solution*. International Journal of Electrochemical Science, 2011. **6**(9): p. 4016-4031.
66. Sherif, E.-S.M., et al., *Corrosion properties in sodium chloride solutions of Al–TiC composites in situ synthesized by HFHF*. Metals, 2015. **5**(4): p. 1799-1811.
67. *Standard Practice for Conventions Applicable to Electrochemical Measurements in Corrosion Testing*.
68. G61-86, A., *Standard Test Method for Conducting Cyclic Potentiodynamic Polarization Measurements for Localized Corrosion Susceptibility of Iron-, Nickel-, or Cobalt-Based Alloys*. 2009.
69. Frankel, G., *Pitting corrosion of metals. A review of the critical factors (vol 145, pg 2186, 1998)*. JOURNAL OF THE ELECTROCHEMICAL SOCIETY, 1998. **145**(8): p. 2970-2970.
70. Touzin, M., *Évaluation de la stabilité d'une couche mince de simili-téflon déposée par plasma sur un substrat d'acier inoxydable*. 2009, Université Laval.
71. Watson, S., et al., *Methods of measuring wear-corrosion synergism*. Wear, 1995. **181**: p. 476-484.
72. Kendig, M. and J. Scully, *Basic aspects of electrochemical impedance application for the life prediction of organic coatings on metals*. Corrosion, 1990. **46**(1): p. 22-29.
73. Castle, J.E. and D.C. Epler, *The correlation of XPS analysis with electrochemical history in aqueous corrosion*. Surface Science, 1975. **53**(1): p. 286-296.
74. Schaeppers, D. and H.H. Strehblow, *An XPS and ISS investigation of passive layers on binary Fe-Al alloys*. Corrosion Science, 1997. **39**(12): p. 2193-2213.
75. Rao, V.S. and V. Raja, *Anodic polarization and surface composition of Fe-16Al-0.14 C alloy in 0.25 M sulfuric acid*. Corrosion, 2003. **59**(7): p. 575-583.
76. Metco, S., *An introduction to thermal spray*. Caderno informativo do fabricante, 2014. **6**.
77. Amin, S. and H. Panchal, *A review on thermal spray coating processes*. transfer, 2016. **2**(4).
78. Amiriyan, M., et al., *Tribo-Mechanical Properties of HVOF Deposited Fe₃Al Coatings Reinforced with TiB₂ Particles for Wear-Resistant Applications*. Materials, 2016. **9**(2): p. 117.
79. Standard, A., *G102-89*. Calculation of corrosion rates and related information from electrochemical measurements, Annual Book of ASTM Standards, ASTM International, Philadelphia, 2004.
80. Standard, A., *G59–97: Standard Test Method for Conducting Potentiodynamic Polarization Resistance Measurements*. Annual Book of ASTM Standards, 2009. **3**.
81. Devos, O., C. Gabrielli, and B. Tribollet, *Simultaneous EIS and in situ microscope observation on a partially blocked electrode application to scale electrodeposition*. Electrochimica Acta, 2006. **51**(8–9): p. 1413-1422.
82. Osório, W.R., E.S. Freitas, and A. Garcia, *EIS and potentiodynamic polarization studies on immiscible monotectic Al–In alloys*. Electrochimica Acta, 2013. **102**: p. 436-445.
83. Jorcin, J.-B., et al., *CPE analysis by local electrochemical impedance spectroscopy*. Electrochimica Acta, 2006. **51**(8): p. 1473-1479.
84. Lavrenko, V.A., et al., *Kinetics and mechanism of electrolytic corrosion of titanium-based ceramics in 3% NaCl solution*. Journal of the European Ceramic Society, 2005. **25**(10): p. 1813-1818.
85. Agarwal, A., M. Akhtar, and R. Balasubramaniam, *Effect of alloying on aqueous corrosion and mechanical behaviour of iron aluminide Fe₃Al*. Journal of materials science, 1996. **31**(19): p. 5207-5213.
86. Sharma, G., et al., *Aqueous Corrosion Behavior of Iron aluminide Intermetallics*. Journal of Materials Engineering and Performance, 2007. **16**(6): p. 779-783.